JOURNAL OF GEOPHYSICAL RESEARCH, VOL. 113, F02012, doi:10.1029/2007JF000872, 2008

Click Here for Full Article

Quantitative morphologic analysis of boulder shape and surface texture to infer environmental history: A case study of rock breakdown at the Ephrata Fan, Channeled Scabland, Washington

Bethany L. Ehlmann,[1] Heather A. Viles,[2] and Mary C. Bourke[2,3]

Received 11 July 2007; revised 2 November 2007; accepted 1 February 2008; published 6 May 2008.

[1] Boulder morphology reflects both lithology and climate and is dictated by the combined effects of erosion, transport, and weathering. At present, morphologic information at the boulder scale is underutilized as a recorder of environmental processes, partly because of the lack of a systematic quantitative parameter set for reporting and comparing data sets. We develop such a parameter set, incorporating a range of measures of boulder form and surface texture. We use standard shape metrics measured in the field and fractal and morphometric classification methods borrowed from landscape analysis and applied to laser-scanned molds. The parameter set was pilot tested on three populations of basalt boulders with distinct breakdown histories in the Channeled Scabland, Washington: (1) basalt outcrop talus; (2) flood-transported boulders recently excavated from a quarry; and (3) flood-transported boulders, extensively weathered in situ on the Ephrata Fan surface. Size and shape data were found to distinguish between flood-transported and untransported boulders. Size and edge angles ($\sim$120°) of flood-transported boulders suggest removal by preferential fracturing along preexisting columnar joints, and curvature data indicate rounding relative to outcrop boulders. Surface textural data show that boulders which have been exposed at the surface are significantly rougher than those buried by fan sediments. Past signatures diagnostic of flood transport still persist on surface boulders, despite ongoing overprinting by processes in the present breakdown environment through roughening and fracturing in situ. Further use of this quantitative boulder parameter set at other terrestrial and planetary sites will aid in cataloging and understanding morphologic signatures of environmental processes.

Citation: Ehlmann, B. L., H. A. Viles, and M. C. Bourke (2008), Quantitative morphologic analysis of boulder shape and surface texture to infer environmental history: A case study of rock breakdown at the Ephrata Fan, Channeled Scabland, Washington, *J. Geophys. Res.*, *113*, F02012, doi:10.1029/2007JF000872.

1. Introduction

[2] Environmental processes leave morphological imprints on rock surfaces at scales from nm to km [*Viles*, 2001]. Many previous studies have used such imprints to infer environmental histories at sand grain [e.g., *Mahaney*, 2002] and landscape [e.g., *Lancaster*, 1995; *Evans and McClean*, 1995; *McClean and Evans*, 2000] scales, but the record provided by boulders has not been well explored. Previous work has tended to focus on size and sorting of boulder populations as evidence of process histories [e.g., *Noormets et al.*, 2002; *Williams*, 1983] or on boulder weathering rinds, hardness and lichen populations as geochronological tools [e.g., *Boelhouwers et al.*, 1999; *Sak et al.*, 2004; *Smith et al.*, 2005]. *Birkeland* [1999] provides a good review of the range of quantitative weathering rate data used in such studies. Boulder morphologies should also provide records of environmental processes, possibly over thousands to millions of years, if signatures in their shape and surface texture can be identified and interpreted. This work develops a comprehensive parameter set for quantifying boulder morphology (size, shape, and texture) and applies this in a pilot study to assess whether boulder populations with different known transport and weathering histories can be distinguished. Our parameter set has applications to planetary environmental histories as well as those on Earth. Landed planetary missions encounter predominantly float rocks, which have no obvious associated outcrop and frequently must rely on these for interpreting environmental history. Recent imaging by the Spirit rover on Mars [e.g., *Arvidson et al.*, 2006], for example, reveals diverse boulder morphologies which could be related to spectroscopic, microscopic and abrasion tool information on the degree and nature of rock breakdown.

[1]Department of Geological Sciences, Brown University, Providence, Rhode Island, USA.
[2]School of Geography and Environment, University of Oxford, Oxford, UK.
[3]Planetary Sciences Institute, Tucson, Arizona, USA.

Copyright 2008 by the American Geophysical Union.
0148-0227/08/2007JF000872$09.00

[3] Rock masses are transformed into soil and sedimentary debris by the combined effects of weathering and erosion. These processes may be collectively referred to as rock breakdown. Boulder morphology is controlled by the interaction between lithology and the particular rock breakdown processes at work, which are largely dictated by climate and tectonic setting. Past environments should thus be recorded by the morphology of boulders. Previous studies have identified specific features as produced by individual breakdown processes, e.g., ventifacts from aeolian abrasion [e.g., *Greeley et al.*, 2002], percussion marks, potholes, incipient cones, and chink facets from fluvial transport [e.g., *Tinkler and Wohl*, 1998; *Bourke and Viles*, 2007]. However, techniques for geomorphological analysis have been mostly qualitative at these centimeter and meter scales, making comparison of boulder shape and texture across locations and between studies difficult at present.

[4] Understanding the uniqueness and persistence of boulder morphological features are two key challenges for improving the utility of boulders as a source of paleoenvironmental information. For example, spheroidal boulders are found in systems with high energy fluvial transport [*Williams*, 1983] but also as corestones in chemically weathered sedimentary strata [*Ryan et al.*, 2005]. Additionally, as the timescales under consideration increase, multiple processes interact, making interpretation of process signatures increasingly difficult. Boulders represent a palimpsest, with signatures of later processes overprinting or destroying earlier morphological imprints. In order to address these challenges replicable methods of describing boulder morphology need to be developed.

[5] Physical parameters for rock breakdown extent are already readily and routinely quantified, e.g., Schmidt hammer rebound values as a proxy for hardness, porosity as a volumetric ratio, rind depth in millimeters. No standardized set of quantitative metrics as yet exists to describe morphology, however. Reporting boulder surface forms still relies largely on qualitative description of surfaces as "pitted," "abraded," and "fractured" without conventions for describing scale, extent, and form. A feature atlas including images, descriptions of morphology, and formation processes has been completed for fluvial, aeolian, and weathering rock breakdown morphologies at the boulder scale [*Bourke and Viles*, 2007]. This allows assessment of the frequency of these features (e.g., by facet mapping [*Heslop et al.*, 2004]), but does not standardize reporting variation in their form or the boulder's general shape. Other studies focus on particular weathering features and their reporting, e.g., cracks [*McFadden et al.*, 2005], tafoni [*Turkington and Phillips*, 2004], or fluvial sculpted forms [*Richardson and Carling*, 2005]. In terms of the general morphology, boulder studies often borrow the semiquantitative, categorical metrics of sphericity and rounding (e.g., those of *Sneed and Folk* [1958], see *Barrett* [1980] for a review) used in sedimentological grain analysis and are usually based on comparison to visual charts. A few researchers move beyond categorical to quantitative indices. *Yingst et al.* [2007] quantify elongation, sphericity and curvature of boulders at the Mars Pathfinder landing site using boulder axis measurements and inscription of circles to boulder perimeters and edges. *Rouai and Dekayir* [2001] and *Yang and Wu* [2006] employ the fractal box-counting method on the perimeter of a 2 d projection of the boulder. *Durian et al.* [2006] image clasts and trace their outlines and find that boulders from different environments have varying statistical distribution of curvatures.

[6] While these measures of size, specific morphology, and shape outline may be sufficient to capture the diversity of sand and gravel-sized particles (<6.4 cm), additional information on rock breakdown processes at the boulder scale can be obtained by more fully examining three dimensional information, including morphologic parameters such as surface texture and the angle of intersection of facets of a boulder. In particular, to parameterize boulder surface texture, the potential exists to borrow and apply tools from other disciplines. Herein, we utilize two techniques from landscape analysis: fractal analysis of surface roughness [*Shepard et al.*, 2001] and morphometric classification of surface forms at multiple scales [*Wood*, 1996] (see section 3).

[7] In the following sections we first develop a quantitative parameter set for reporting boulder size, shape and texture. We then test the ability of this parameter set alongside standard methods to distinguish three boulder populations in the Channeled Scabland which have well-constrained and different environmental histories. The degree to which boulder morphology is diagnostic of rock breakdown process and extent is considered.

2. Study Site

[8] To study the effects of distinct breakdown processes in shaping boulder morphology, we required a site for which we had (1) extensive a priori knowledge of its geology and geomorphic history; (2) distinct groups of boulders with well-constrained but divergent rock breakdown histories; and (3) boulders of similar lithology in order to control its effects on boulder form and thereby isolate the effects of geomorphic processes. The Ephrata Fan in the Channeled Scabland of eastern Washington (47°20′N, 119°30′W, Figure 1) is particularly well suited to fulfilling these criteria. Additionally, the Channeled Scabland megaflood site has planetary science relevance: it has long been recognized as an analog for large outflow channels on Mars similar to Ares Vallis and the Mars Pathfinder landing site [e.g., *Golombek and Rapp*, 1997] and Columbia River basalt is geochemically similar to some basalt on Mars [*Wyatt and McSween*, 2002].

2.1. Geology and Boulder Lithology

[9] The Ephrata Fan is dominated by boulders of the Columbia River Basalts (CRB), a 20,000 km^2 layered continental flood basalt sequence up to 1 km thick, 98% of which was deposited in a series of eruptions between 16.5 and 14.5 Ma BP [*Swanson and Wright*, 1978]. CRB flows are rich in labradorite, plagioclase, augite, pigeonite, and occasionally Fe-rich olivine [*Hooper et al.*, 2007]. Outcrops near our site at the southern end of Grand Coulee contain the Lookingglass and Frenchman Springs members of the Wanapum formation which are undifferentiated fine grained to aphanitic flow units with hackly columnar jointing (Figure 1b) [*Grolier and Bingham*, 1971; *Swanson et al.*, 1979; *Hooper et al.*, 2007].

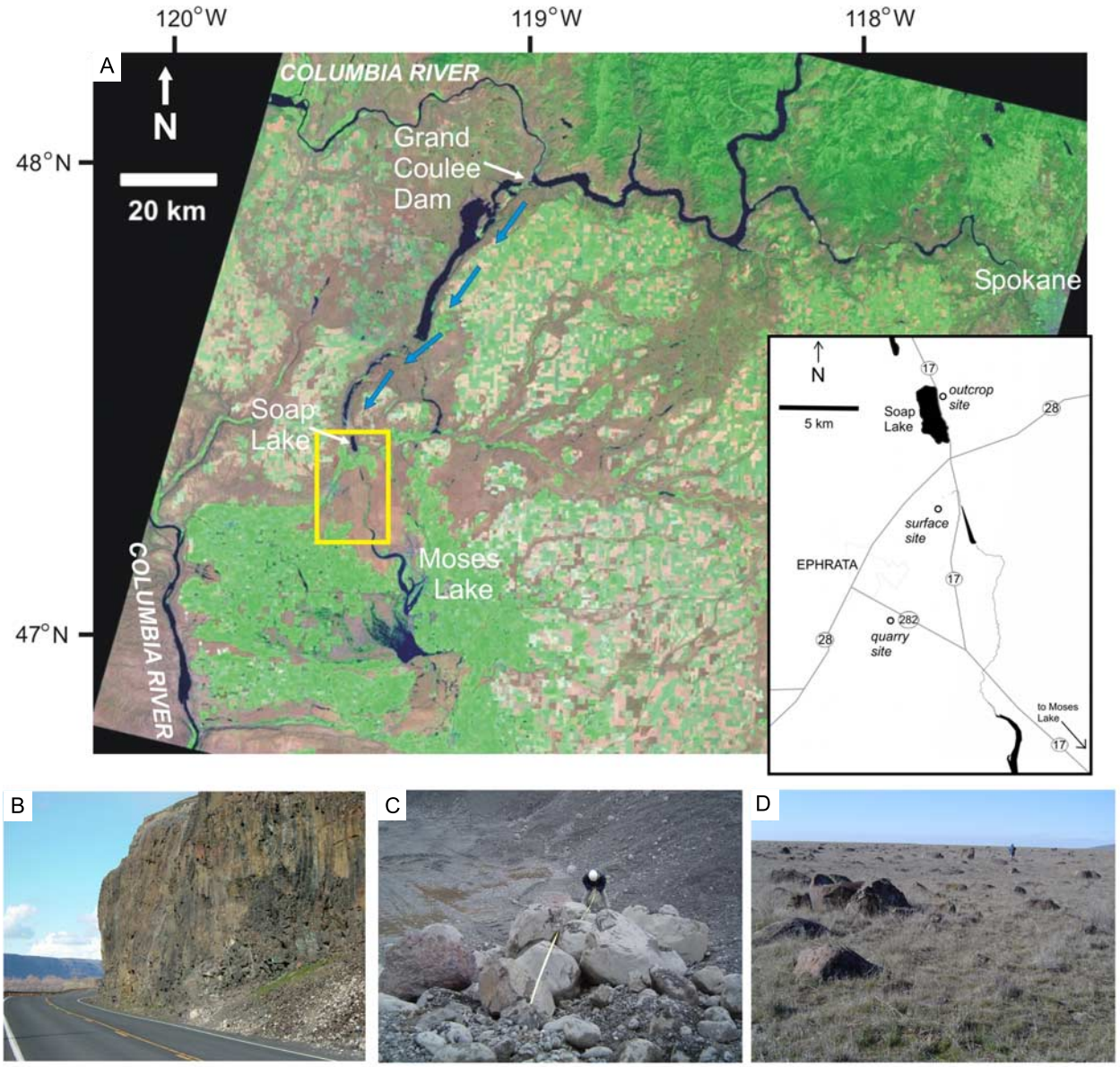

Figure 1. (a) False color Landsat image (bands 5, 4, and 3 are red, green, and blue, respectively, image ELP044R027_7T19990723) of the Channeled Scabland. Arrows indicate the path of floodwaters through Grand Coulee during the last Lake Missoula breakout event. The Ephrata Fan boulder deposits at the distal end can be recognized on the satellite image by the lack of agricultural fields. Box indicates the location of the inset, a schematic map of the locations of sampling sites. (b) Basalt outcrop at the eastern shore of Soap Lake with vertical columnar jointing. (c) Boulders piled during excavation at the Ephrata gravel quarry site, and (d) the Ephrata Fan boulder field at the surface site.

[10] Crystalinity, vesicularity, and composition vary relatively little between flow units, allowing the first-order assumption that intersite and intrasite differences in parent flow unit are of negligible importance to breakdown processes and morphology of boulders of the CRB [*Hooper*, 2000]. The greatest source of variation is the stratigraphic location of source rock within a flow unit. Differences in depth during cooling and consequent fracturing created a classic stratigraphy found in numerous basalt flows: a basal pillow-palagonite complex overlain by a "colonnade" unit of well-ordered hexagonal columns, capped by a less-ordered "entablature" of irregular columns and additional cooling fractures [*Long and Wood*, 1986; *Aydin and Degraff*, 1988].

2.2. Quaternary Geomorphic History and Climate

[11] Loess and alluvial deposits from glacial outwash were deposited over the CRB in the Quaternary, and 17,000–12,000 years ago, the Columbia and Snake River plains were reshaped in a series of outburst floods from glacial Lake Missoula [*Bretz*, 1923; *Baker and Nummedal*,

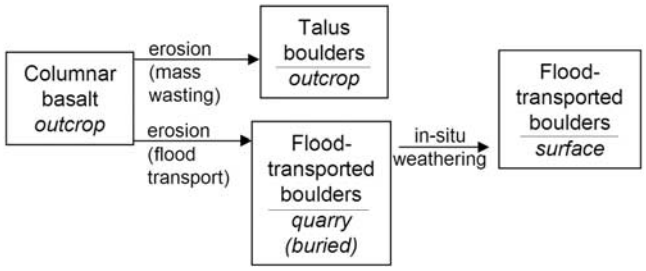

Figure 2. Rock breakdown sequence at the Ephrata Fan. Boulders at the base of the outcrop are $\sim 10^1 - 10^2$ year old talus. Quarry and surface boulders underwent flood transport and were, respectively, buried and removed from the surface environment or exposed to the surface weathering environment for $\sim 10^4$ years.

1978; *Clague et al.*, 2003]. Preexisting soils and glacial debris were removed creating the Channeled Scabland morphology of kilometer scale scoured channel systems, megaripples, and large boulder bars [*Baker*, 1978a]. The Ephrata Fan, our study site, is at the distal end of Grand Coulee where during the most recent episode of flooding, waters exiting the coulee decelerated, depositing their sediment load in a subaqueous fan extending approximately 800 km^2 (Figure 1a) [*Bretz*, 1923]. Boulder-sized objects near the mouth of the coulee fine southward, away from the mouth, to sand-sized sediments which have been reworked into the Moses Lake dune field [*Rice and Edgett*, 1997]. The 10 km of the Ephrata Fan closest to Soap Lake has a notable concentration of boulders due to erosion of fines during late stage drainage of the basin [*Golombek and Rapp*, 1997]. Approximately 90% of the boulders are basalt, derived from the Columbia River flood basalts [*Rice and Edgett*, 1997; our field observations]. In some places boulders are overlain by flood transported sediments [*Swanson and Wright*, 1978].

[12] From ~10 ka BP, grasslands have dominated eastern Washington, and all data suggest a continuously cool and dry climate since the Lake Missoula floods [*Mehringer*, 1985]. Human agriculture and aeolian reworking of flood sediments and glacial loess have been the most active geomorphic processes since the last Scabland flood [*Rice and Edgett*, 1997]. Present-day average precipitation is less than 20 cm. Average daily temperature range in the summer is 15 to 30°C and during the winter is −5.5 to 1°C (National Weather Service, Observed data for Ephrata, 1950–2005, Cooperative Observer Data, National Weather Service Forecast Office, Spokane, Washington, accessed 2 August 2006, available at http://www.wrh.noaa. gov/otx/climate/coop/coop.php).

2.3. Field Locations for Boulder Sampling

[13] Three boulder sampling sites were identified: surface, quarry, and outcrop (Figures 1b–1d). The surface site is a field of exposed boulders on the Ephrata fan surface. The quarry site is a large open pit dug into the Scabland flood-transported sediments on the southern end of the Ephrata Fan. These are being mined for concrete production. The outcrop site is located in the basalt cliffs along the eastern shore of Soap Lake. Care was taken to select an outcrop where the colonnade structure was readily apparent.

[14] We hypothesize that each of these sampling sites represents a different path taken in the rock breakdown process (Figure 2). This allows certain assumptions to be made regarding the types and timescales of processes which have acted on the boulders at each of the sites and which can be related to their morphology. Quarry boulders were transported in the Lake Missoula flood events (between 12,000 and 17,000 years ago) and were buried immediately by finer debris as floodwaters receded. Thus protected from the subaerial weathering environment, they should represent boulders with a clear flood transport imprint and little subsequent alteration. This assumes burial in alluvium does not enhance weathering, an appropriate assumption given that soils of semiarid Eastern Washington form well above the water table and do not have well-defined horizons. *Birkeland* [1999, p. 172] noted a similar lack of weathering of buried granite boulders in <20,000 year old tills in California. Boulders from the Ephrata fan surface have experienced flood transport followed by exposure to the Ephrata surface weathering environment for up to 12,000 years. From the climate of the area, we hypothesize rock breakdown to be dominated by freeze-thaw and/or thermal cycling, chemical oxidation of iron bearing minerals, and lichen-induced biological weathering. We assume both quarry and surface boulders are unlikely to have inherited preflood transport weathering features since the high energy transport would have erased any surface signatures. Boulders from the outcrop represent a different breakdown path whose time of exposure is not as well constrained but is probably no more than $\sim 10^2$ years (as boulders). This corresponds to the approximate time of construction of Soap Lake Road (Route 17) when boulders were likely cleared from the base of the outcrop (Figure 1). Boulders at the outcrop site have not experienced transport but have simply detached from the outcrop and remained at its base. In addition to lack of fluvial transport, the method of detachment also may differ from flood transported boulders, e.g., mass wasting following weakening by freeze-thaw or chemical weathering as opposed to cavitation and plucking and abrasion. Outcrop boulders will also have experienced in situ weathering, like the fan surface boulders; however, the time span available for such weathering is likely at least an order of magnitude less than for the fan surface boulders. Furthermore, unlike the quarry and fan surface boulders the outcrop boulders may have inherited features from in situ alteration, such as caused by percolating reactive fluids within joint systems.

3. Methods

[15] For each of the three boulder sites, measurements were made to characterize the extent and characteristics of rock breakdown experienced by boulders, boulder morphology, and boulder surface texture. Specific quantitative parameters measured are listed in Table 1. At each sampling site, 10–50 boulders were selected for measurement and 10 samples were chosen for casting so that detailed laser scanning could be undertaken in the laboratory. Boulders were chosen by laying a transect and, at intervals, selecting the nearest boulder. Quantitative parameters were compared

Table 1. Summary of Methods Used in the Ephrata Boulder Study[a]

Breakdown Extent	Boulder Shape	Boulder Surface Texture
Number of fractures and detached blocks	*Axes length measurement*	Molding and laser scanning to generate surface digital elevation models (DEMs)
Percentage lichen cover estimation	Shape parameter calculation using *Sneed and Folk*'s [1958] sedimentological classification	Fractal analysis of roughness scaling behavior (*RMS height and deviation, H, breakpoints*)
Schmidt hammer rebound	Edge profiling to calculate *facet angle* and *radius of curvature ratio*	*Morphometric classification at multiple scales*
Thin section petrographic texture analysis		
Measurement of weathering rind depth		

[a]Italics indicate the measurement is part of the quantitative morphologic parameter set whose effectiveness was tested by this study.

between sites using the two-tailed t test; equal variances were not assumed.

3.1. Assessing the Extent of Rock Breakdown

[16] To verify that the extent and type of rock breakdown processes experienced by boulders at each site matched our expectations based on the overall geologic history of region, samples were collected for subsequent laboratory analysis and measurements made in the field. In the field fractures, lichen cover, and surface hardness were recorded as described below. Boulder surfaces were examined for fractures, whose number and length were recorded. Some fractures may have been obscured by lichen cover. Partially and completely detached pieces of the boulder were identified and measured. Percentage lichen cover across whole boulders and individual facets was estimated independently by two workers and an agreed figure recorded. A Schmidt rebound hammer was used to test surface mechanical strength. Measured rebound values are highly correlated with surface hardness which is in turn related to mechanical strength [*Day and Goudie*, 1977]. Ten hammer measurements were taken on each surface and values averaged. There are known limitations to the Schmidt hammer technique: rebound values are suspect on small, weak, fractured, or nonhomogenous rocks [*Dincer et al.*, 2004]. They also vary with moisture [*Sumner and Nel*, 2002] and are influenced by surface texture irregularities [*Williams and Robinson*, 1983; *McCarroll*, 1991]. In order to minimize errors from these factors we only sampled boulders with all axes >15 cm, pretreated the surfaces with carborundum, avoided heavily lichen-covered surfaces when possible and sampled under similar weather conditions.

[17] At least three samples were taken at each site for further laboratory analysis of the extent of weathering. Surfaces and cross sections of hand samples were examined with an optical microscope and thin sections were made, following impregnation in blue resin to minimize damage to potential weathering rinds and highlight porosity in the rock [*Curran et al.*, 2002; *Gordon and Dorn*, 2005]. These were then examined using a petrographic microscope for identification of constituent minerals and estimation of the depth of weathering.

3.2. Morphologic Statistics: Whole Boulder Size and Shape

[18] Photographs and field measurements were made in order to characterize boulder size, shape, and specific breakdown features. The principal boulder axes were measured, shape parameters calculated, and angularity and curvature of edges between facets recorded as described below.

[19] Long, intermediate, and short axes of the boulders were measured easily for outcrop and quarry samples where the entire boulder was visible. Some surface site boulders were partially buried by soil and grasses, and in such cases, soil was excavated on one side of the boulder until a trowel could undercut the boulder. Height to the undercut was measured. This may have resulted in underestimation of surface boulder heights, and measured values represent lower limits. For comparison of boulders to outcrop columns, photographs and column width measurements were taken every 5 m along the outcrop to characterize outcrop fracture patterns for comparison to boulder size.

[20] To assess boulder shape using standard sedimentological criteria, maximum projection sphericity (ψ), deviation from compactness (D), and the form factor (F) were calculated from axis measurements according to the respective formulae

$$\psi = \sqrt[3]{\frac{S^2}{LI}}, \tag{1}$$

$$D = \frac{S}{L}, \tag{2}$$

$$F = \frac{L - I}{L - S}, \tag{3}$$

where L, I, and S are the boulder's long, intermediate, and short axes [*Sneed and Folk*, 1958]. Values for these parameters range from 0 to 1. Maximum projection sphericity is defined as the ratio between the maximum projection area of a sphere with the same volume as the particle and the maximum projection area of the particle. Combined with the form factor and compactness, this allows form fields to be defined in which particles are compact, platy, bladed, or elongate (see section 3, Figure 8).

[21] To measure angularity and curvature of facet edges, a 40 cm carpenter's profile gauge was used to record a profile of boulder edges by pressing a row of pins, each 0.16 cm thick, against the meeting point of two facets. This was then traced to record the shape (Figure 3). Angle of the contact

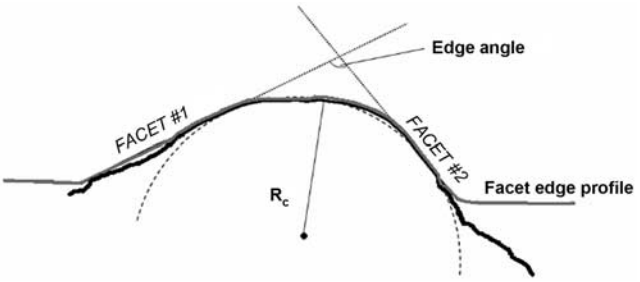

Figure 3. Profile of the edge at which two boulder facets meet (gray). Note that the gauge was not in contact with the surface at the beginning and end of the profile. The boulder outline is shown in black. The edge angle parameter is the interior angle at the intersection of two best fit lines to the facet faces. R_c denotes the radius of curvature and is the radius of the largest circle which can be inscribed in the facet edge.

and radius of curvature were calculated from best fits to the trace of the profile. This was done for three facet edges on each boulder. Radius of curvature values are reported as a ratio of R_c/R_a where R_c is the radius of the largest circle that can be inscribed within the natural curve of the boulder surface at the meeting point of the facet edges and R_a is the average radius of the boulder. Similar relative curvature measures have also been employed by *Durian et al.* [2006]. In this case, because of the uncertainty in height of surface boulders, we used only the other two axes in all cases to calculate R_a in the radius of curvature ratio. The curvature ratio will yield a value of 1 if the profile is taken from a sphere and 0 if taken from a perpendicular edge, e.g., from a cube, or other sharp edge such as that formed by two concave facets.

3.3. Morphological Statistics: Surface Texture Analysis

[22] In order to quantify surface texture a digital model from which boulder surface roughness and surface morphology could be analyzed quantitatively was required, however, boulders were too large for transport and laser scanning in the field was not possible. Use of molding and casting to capture detail of surfaces is a well-established method for recording archeological artifacts and sedimentary surfaces [e.g., *Dowman*, 1970; *Buffin-Bélanger et al.*, 2003] and a similar technique, using plaster of paris, was used here.

[23] At each field sampling site, 10 boulders with relatively horizontal facets of at least 15 × 15 cm were selected. This minimum size was necessary to ensure sufficient area for computing statistics for quantitative parameters measuring surface texture. The boulder surface was brushed clean and sprayed with an oil-based separator. Plaster of Paris was mixed and applied in a ~2 cm thick layer atop the boulder. After drying for approximately 30 min, the mold was removed. In the laboratory, whole molds were scanned at a minimum resolution of 0.4–0.7 mm point separation with a Konica Minolta VI-9i three-dimensional digitizer. A 10 × 10 cm subset of each mold was scanned at 0.2 mm resolution. Any losses in horizontal and vertical resolution of the impression of the surface induced by the casting technique were determined by scanning the surface of a control boulder in the laboratory, taking a mold, and then scanning the mold and the rock postmold. The boulder chosen was composed of sandstone but was similar in surface texture to the Ephrata basalt boulders. The control rock had a smooth, fine-grained surface, a portion of which was covered by lichen so we could assess its effects on the molding process.

[24] Prior to analysis, raw x, y, z point data from scanning were detrended, processed into raster format using a smooth quintic polynomial interpolation, and then inverted to reflect the topography of the original boulder surface rather than the mold. At the end of this preprocessing, a regularly spaced gridded array of boulder surface elevation values was obtained. Elevation was relative to a mean z value for the surface. With this digital elevation model of the surface, systematic investigation of surface texture via fractal analysis and morphometric classification could be performed.

3.3.1. Fractal Analysis of Roughness Scaling

[25] Fractal analysis considers the scaling behavior of topographic surface roughness. For this study, following the conventions argued for by *Shepard et al.* [2001], three fractal parameters were reported to characterize the surface roughness and roughness scaling of boulders: Root mean square (RMS) height, RMS deviation, and the Hurst exponent (H), including breakpoints in H. RMS height (ξ) is the standard deviation of heights above the mean for a given sample area according to the equation

$$\xi = \left(\frac{1}{n-1} \sum_{i=1}^{n} (z(x_i, y_i) - \bar{z})^2 \right)^{1/2},$$

where n is the number of sample points in the area under consideration, $z(x_i, y_i)$ is the height of the surface at point (x_i, y_i), and $\bar{z}$ is the mean height of over all x, y. RMS height is calculated for the whole sample or over a selected window size. High RMS height values indicate rough surfaces, since points in a given sampling window show large deviation from the mean value.

[26] A similar measure, RMS deviation, reports the height difference between points separated by a lag or step Δd and is calculated

$$v(\Delta d) = \left(\frac{1}{n} \sum_{i=1}^{n} [z(x_i, y_i) - z(x_i + \Delta x, y_i + \Delta y)]^2 \right)^{1/2},$$

where n is the number of sample points in the sample, $z(x_i, y_i)$ is the height of the surface at point (x_i, y_i), and $z(x_i + \Delta x, y + \Delta y)$ is the height of the surface at a distance $\Delta d = \sqrt{\Delta x^2 + \Delta y^2}$ from (x_i, y_i). (RMS deviation is also sometimes reported as RMS slope $\theta(\Delta d) = \tan^{-1}(v(\Delta d)/\Delta d)$). High values correspond to greater roughness, i.e., adjacent points show steep elevation differences.

[27] Surface roughness as measured by RMS height and RMS slope varies as a function of scale [*Turcotte*, 1997], and for natural surfaces, the vertical scale, elevation, does not increase as quickly as the horizontal scale increases in size [*Shepard et al.*, 1995]. Instead the increase with scale follows a power law relationship whose slope, H, in a log-log plot relates to the surface roughness scaling. H, also known as the Hurst exponent, usually varies from 0 to 1.

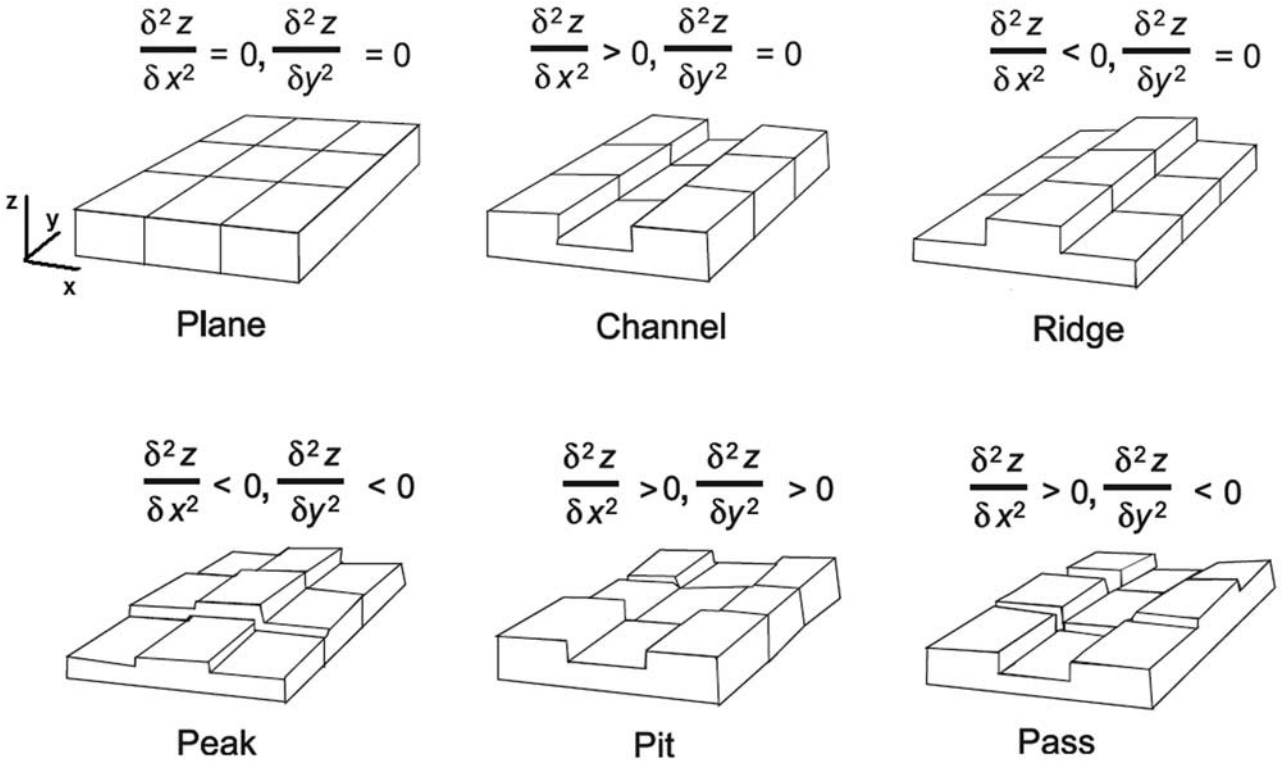

Figure 4. The six morphometric classes as defined by the second derivatives in the x and y directions. Classes are shown for a window size of 3 × 3 pixels. (Modified from *Wood* [1996] and *Bolongaro-Crevenna et al.* [2005].)

That is, the values for RMS height or RMS deviation scale as

$$\xi(L) = \xi_0 L^H$$
or
$$v(\Delta d) = v_0(\Delta d)^H.$$

These values of H are obtained from a variogram, a log-log plot of RMS deviation as a function of point to point distance. Low H values mean terrain smoothes rapidly as scale increases while high values indicate the surface maintains its roughness. Natural surfaces at the landscape scale typically have H values ~0.5, although many surfaces display "breakpoints" in scaling behavior where different H values apply over different scales. This is thought to be due to the dominance of different geomorphic processes at different spatial scales [*Shepard et al.*, 2001; *McClean and Evans*, 2000].

[28] For this study, RMS height and RMS deviation were calculated over multiple scales for boulder mold surfaces and deviogram log-log plots were produced. To ensure a sufficient number of independent samples, statistics were computed only from the sampling interval up to no more than 1/10th the scale of the entire surface. Using deviograms, breakpoints were identified and slopes evaluated to obtain H values of fractal scaling behavior. RMS deviation is reported at 1 mm and 1 cm intervals while RMS height is reported over square windows of side length 1 mm and 1 cm (areas 1 mm^2 and 1 cm^2).

3.3.2. Morphometric Classification of Geomorphic Features

[29] Surface relief can be described by the occurrence of distinct landforms [*Fisher et al.*, 2004; *Bolongaro-Crevenna et al.*, 2005]. *Wood* [1996] developed a methodology for landscape analysis of digital elevation models (DEMs) by creating a six class set of simple, mathematical morphometric forms: ridge, channel, plane, peak, pit, and pass. The numerical representations of these forms are based on the second derivatives in orthogonal directions at the central point over a given window size (Figure 4). Window sizes can be 3 × 3 pixels, 5 × 5 pixels, or greater to calculate the frequency of these morphometric forms at different spatial scales. These surface forms can be mapped on a digital elevation model (Figure 5).

[30] Each morphometric form is a "landform" which in the context of analysis of a boulder surface may correspond to a specific surface feature, e.g., a peak of a protruding phenocryst, a pit caused by impacts during fluvial transport, or channel-like depressions left by dissolution as water flows over a boulder surface. Morphometric class distribution may be related to the rock breakdown processes acting on the surface. The distribution of feature classes present in a landscape varies as a function of the scale of observation. To investigate such scaling behavior, we computed feature classification for a set of window sizes appropriate to the resolution of the digital elevation surface model and the size of the sample. Using *Wood*'s [1996] methodology and software (LandSerf, version 2.2, 2006, Copyright J. Wood 1996–2005, downloaded November 2005, available at

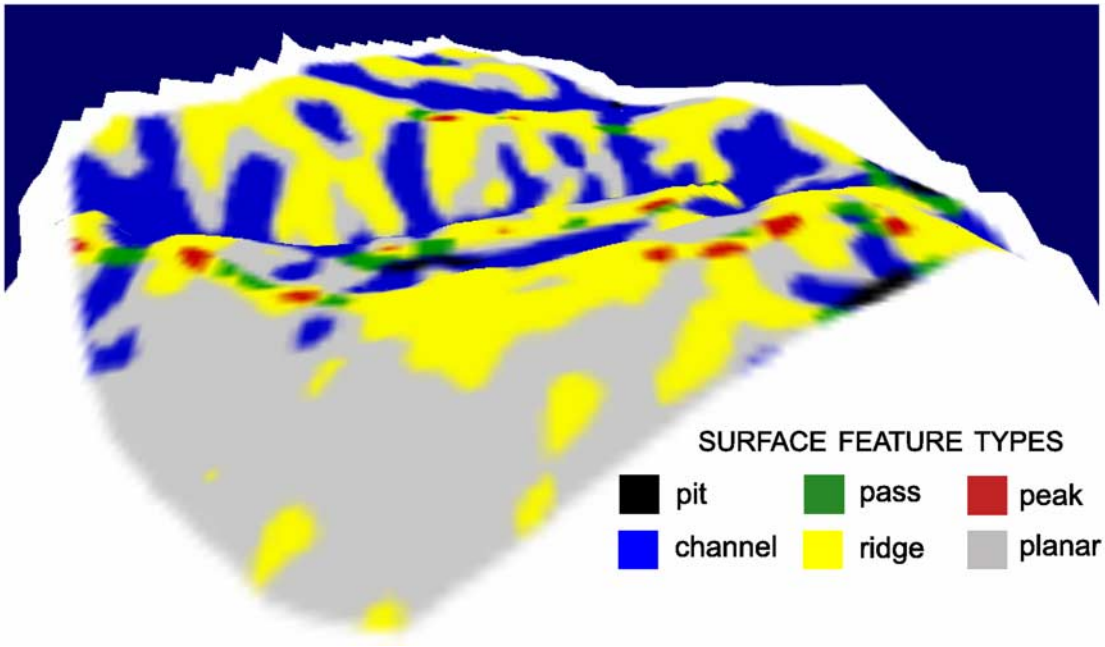

Figure 5. Morphometric classification at the 1 cm scale draped over the digital elevation model of the boulder mold from boulder Q5 at the quarry. The central trough in the image is from a large conchoidal fracture. Relief is approximately 2 cm, and the cast is approximately 13 × 15 cm.

http://www.landserf.org), percent frequency of each morphometric form was calculated for each boulder surface mold using several window scale sizes, 3 × 3 and higher. Reported morphometric class frequencies are for windows of side length ~1.5 mm (3 × 3 at the limit of resolution, ~0.5 mm as discussed below), 1, 3, and 5 cm for the 225 cm^2 molds. Threshold values of slope and curvature of 5.0 and 0.1 were used as suggested by *Fisher et al.* [2004]. Once morphometric classes were determined for each boulder, frequency percentages were computed and compared for boulders at the three sites at different scales.

4. Results

4.1. Extent of Rock Breakdown

[31] The appearance of boulders varied greatly between the three sites (Figure 6). Boulders in the quarry had pristine flood transport related features readily observable on the light gray surfaces. These included percussion fracture facets, fissures, and incipient cones (Figure 6a) [*Bourke and Viles*, 2007]. Approximately two-thirds of the quarry boulders had small, less than 1 mm wide fractures on the surface, and slightly less than half had multiple fractures including some as long as 100 cm. Lichen was completely absent from quarry boulders.

[32] Interestingly, on surface boulders, lichen tended to obscure percussion fracture facets and other fluvial features which form topographic lows by preferentially colonizing them. While fractures were difficult to identify because of lichen cover, 6 of 20 surface boulders had at least one large (>10 × 10 cm) detached rock fragment adjacent to the largest boulder fragment (Table 2, Figure 6d). These indicate in situ fracturing. On fan surface boulders, lichen coverage on a whole boulder basis varied from 30 to 100%. On a smaller scale, patchiness was evident with lichen coverage on a per facet basis varying from 10 to 100% even on a single boulder. Boulders were reddish-brown in color.

[33] At the outcrop site, boulders had few fractures on the surface; all measured less than 30 cm in length. Some cracks were wider than those at the quarry site, measuring from a few millimeters to 1.5 cm in width. Three boulders had small detached fragments. Observation of columns at the outcrop site showed numerous fractures perpendicular to hexagonal columnar jointing (Figure 6c) and locations from which some boulders fell could be identified. Fresh surfaces recently exposed by rockfall were darker in color than the surrounding brownish outcrop, indicating some oxidative weathering of the outcrop occurs prior to boulder formation. Lichen was found only rarely on outcrop boulders.

[34] In terms of physical hardness, the Schmidt hammer data reveal significant differences between the three sites at the $p < 0.05$ level (Table 2). Quarry boulders had the highest rebound values (65.2 ± 4.6), and surface boulders had the lowest (55.9 ± 8.6). Surface boulders also show the greatest variation in Schmidt hammer values. Outcrop boulders are slightly harder than surface boulders and with slightly less variation (58.4 ± 7.1). Hardness varies by lichen coverage as well as by site. Facets of surface boulders with >80% lichen cover (51 ± 10.0) were significantly softer than facets with <50% lichen cover (56 ± 11.2). No correlation was found with boulder size or number of fractures/detachments, though as noted already identification of fractures was hindered on surface boulders because of lichen cover.

[35] Petrographic microscope analyses give some greater insights into the breakdown processes. Morphologically, there are stark differences between sites in the near surface mineral grains of the boulders at millimeter to micron scale when viewed in cross section in the petrographic thin

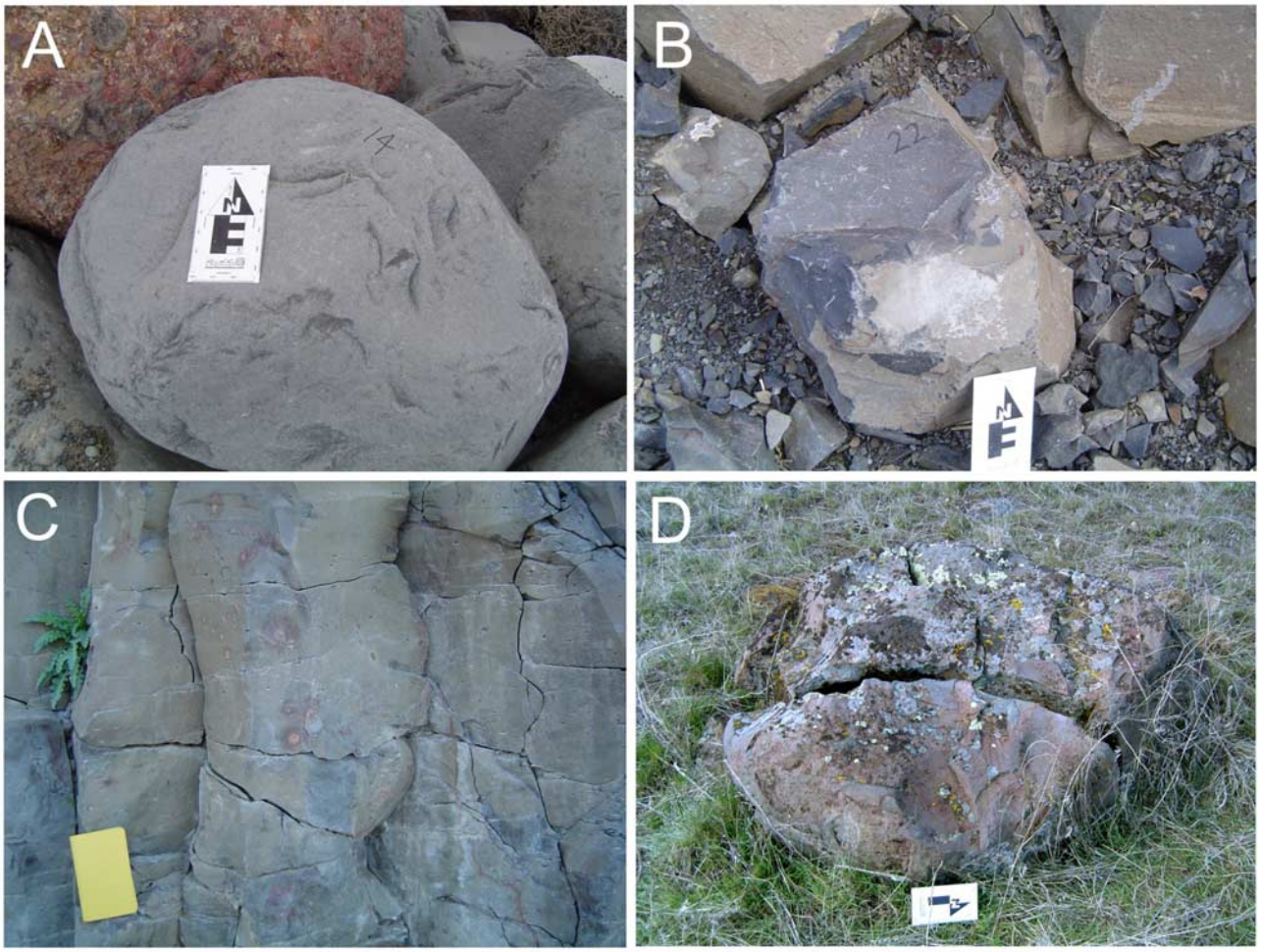

Figure 6. (a) Rounded flood-transported boulder at the quarry site with obvious gouges from flood transport. (b) Angular talus fall boulder at the outcrop site, (c) columnar jointing and perpendicular fracturing on the outcrop face, and (d) boulders exposed at the surface have flood transport features partly obscured by lichen. Detached blocks indicate in situ fracturing. Items for scale in the images are approximately 12 cm.

sections (Figure 7). Quarry boulders have smooth surface-grain interfaces. In contrast, samples from the outcrop have jagged surface-grain interfaces, perhaps because of the effects of granular disintegration. In the fan surface samples, the uppermost layer of grains is highly fractured and in some cases the root-like rhizines of lichen penetrate individual grains. Grain fracturing and red iron oxidation are the most obvious signs of weathering, forming a clear rind. Iron oxidation was absent from the quarry samples but occurred frequently in the outcrop and surface samples either immediately at the surface in a distinct zone of weathering or at depths of a few mm, perhaps because of infiltration of water in subsurface cracks. Iron oxidation appears to be intensified beneath some lichen.

4.2. Morphologic Parameters: Whole Boulder Shape

[36] Examination of whole boulder shape parameters shows some significant differences between boulders at

Table 2. Boulder Breakdown Extent Statistics and Averages per Boulder[a]

		Per Boulder			
	N Sampled	Average Number of Fractures	Average Number of Fractures Above 15 cm	Average Number of Detached Fragments	Schmidt Hammer Rebound
Quarry boulders	15	2.2 ± 2.9	0.9	0	65.2 ± 4.6
Outcrop boulders	11	1.2 ± 1.6	0.3	0.3	58.4 ± 7.1
Surface boulders	20	0.3 ± 0.4	0.2	1.1	55.9 ± 7.1

[a]Values given are mean standard (±standard deviation).

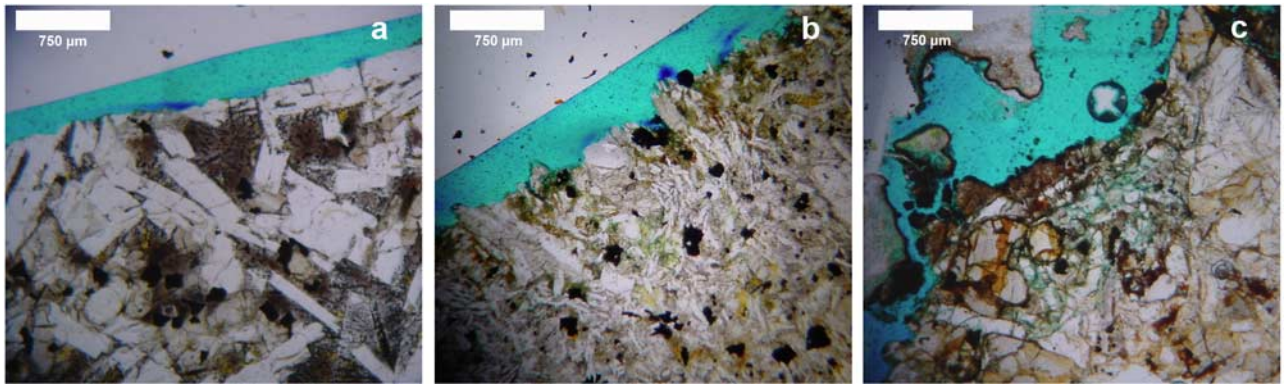

Figure 7. Petrographic thin sections from (a) a quarry boulder, (b) an outcrop boulder, and (c) a surface boulder with lichen cover. At the grain scale the surface interface of the blue resin with the quarry boulder is smooth while the jagged interface on the outcrop boulder may result from granular disintegration. For the surface boulder, resin penetrates into fractures beneath lichen and oxidation of iron-bearing minerals is evident.

the different sites. Volumetrically, boulders in the quarry (0.25 ± 0.18 m^3) are larger than those on the surface (0.16 ± 0.17 m^3) which in turn are significantly larger than those from outcrop talus slopes (0.04 ± 0.03 m^3). However, volumetric differences between the quarry and surface are likely due to measurement technique, i.e., underestimation of buried surface boulder height due to insufficient excavation when taking measurements. When only the boulder long axis is considered, differences between the quarry and surface boulders are negligible, with long axes of 79 ± 26 and 81 ± 44 cm, respectively (Table 3). This is comparable to the average measured width of basalt columns at the outcrop site, 74 ± 57 cm. Average outcrop boulder long axis is 40.5 ± 11 cm, significantly different from the other two locations and from the columns ($p < 0.01$).

[37] Average sphericity of boulders ranged from 0.7 to 0.9. Compactness was 0.5–0.7 and form factor 0.35–0.5. Boulders at all sites are generally compact to subcompact (Table 3, Figure 8). For shape parameters, the only significant difference in boulders at the three sites was in sphericity and compactness of the surface boulders relative to the quarry boulders; however, this is likely to be an effect of systematic underestimation of surface boulder height due to their partial burial.

[38] For the quarry boulders, the average angle at which facets met was $115° \pm 12°$. Average angles for surface and outcrop boulders were $109° \pm 15°$ and $102° \pm 11°$, respectively (Figure 9, Table 3). Surface and quarry samples were not statistically different; however, outcrop boulders were significantly different from both. Surface sample mean is shifted to smaller angles by a tail of low values (Figure 9a).

[39] Differences in the radius of curvature ratio were not statistically significant between quarry (0.13 ± 0.06) and surface (0.14 ± 0.11) boulders (Table 3, Figure 9b). There are obvious and significant differences in curvature between the flood-transported boulders and outcrop talus (0.02 ± 0.02 cm). Surface boulders have a greater range in values, nearly spanning the range found on boulders at the other two sites.

4.3. Morphological Statistics: Surface Texture Analysis

[40] Horizontal resolution of the molding technique is ~1:1, however, vertical resolution of the molding technique for whole surface samples is no more than 500 μm as determined by scanning test rock surfaces and molds of the same area and comparing profiles of the resultant digitized surfaces (Figure 10). Reproductions of the original rock surface are high fidelity for clean, smoothly curving areas. However, in areas with lichen coverage, plaster tended to stick to the rock or to the lichen. In these isolated patches, discrepancies between rock surface and mold may exceed 2 mm. Fortunately, for most molded surfaces, lichen covered less than 10% of the surface area so their overall impact is minimal.

[41] Because of a loss in vertical resolution in the plaster surface model relative to the original rock (500 μm instead

Table 3. Boulder Form Statistics

	N Sampled	Long Axis, cm	Sphericity	Deviation From Compact	Form Factor	Radius of Curvature Ratio	Facet Edge Angle, °
Quarry boulders (Q)	25	78.5 ± 25.6	0.82 ± 0.09	0.68 ± 0.17	0.37 ± 0.31	0.13 ± 0.06	115 ± 12
Surface boulders (S)	46	80.6 ± 44.4	0.69 ± 0.14[b]	0.51 ± 0.18[b]	0.47 ± 0.25[b]	0.14 ± 0.11	109 ± 15
Outcrop boulders (O)	11	40.5 ± 10.9	0.77 ± 0.09	0.62 ± 0.13	0.44 ± 0.34	0.02 ± 0.02	102 ± 11
Outcrop columns (C)	24	74.2 ± 56.8	–	–	–	–	–
Significant differences[a]		O-S, O-Q, O-C	[b]	[b]	[b]	O-S, O-Q	O-S, O-Q

[a]Comparisons were made using a two-tailed t test, without assumed equal variances. Significant differences are reported when $p > 0.05$.
[b]Systematic underestimation of surface boulder short axes biases these parameters. No significant differences were found between the quarry and outcrop boulders.

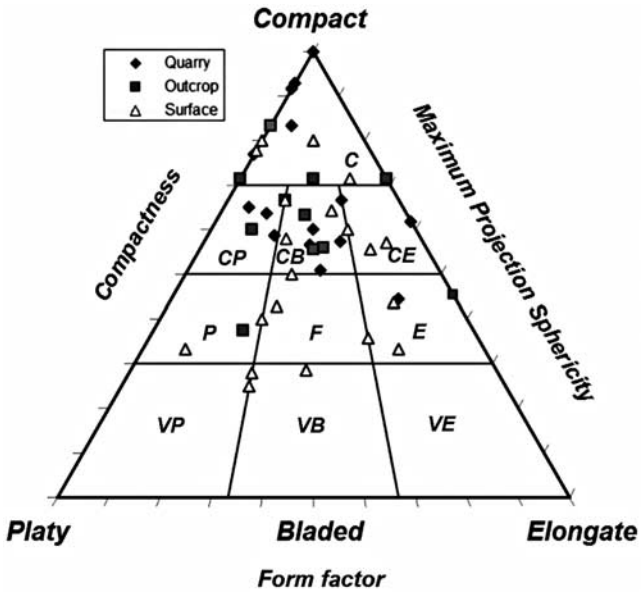

Figure 8. Channeled Scabland boulder data plotted on a *Sneed and Folk* [1958] particle shape diagram (C, compact; P, platy; B, bladed; E, elongate; V, very). Values for each parameter range from 0 to 1. Most boulders plot in the compact field and no site-to-site significant differences are apparent. Note that surface boulder data is likely affected by systematic underestimation of the short axis as discussed in the text (plot produced using the software of *Graham and Midgley* [2000]).

of the 200 μm scan resolution), molds will display less roughness, in absolute terms, than the corresponding actual rock surface. This behavior was characterized by computing and comparing roughness statistics at multiple scales for an actual rock surface, a mold of the surface, and the rock surface postcasting (Figure 10). Plotting a deviogram of step size versus change in height reveals that in absolute terms, the mold is 25% less rough than the actual rock surface. The rock itself, postmolding, was 16% less rough than the original surface. There is no scale dependency of reduction in roughness, i.e., RMS height and RMS deviation reduction is the same percentage when considering millimeter or centimeter scales. Thus, the Hurst exponent and breakpoint scale should not be affected in fractal analysis and relative roughness comparisons between the sites can be made.

[42] Results show that quarry boulders are the smoothest and surface boulders are the roughest. This is true regardless of the scale considered and whether the parameter used to measure roughness is RMS height or RMS slope (Table 4). Surface boulders and outcrop boulders have relatively similar roughness while quarry boulders are obviously different from both. Small sample size (10) and a high degree of variance mean most differences are not statistically significant, although the greater surface boulder RMS height versus that of the quarry is statistically significant at the $p < 0.05$ level for both scale sizes. RMS height plots did not show breakpoints (probably because only small scales were considered in order to have sufficient independent samples), though boulder RMS deviation deviograms exhibit breakpoints which differed between the sites (Table 5, Figure 11). Outcrop boulder deviograms had breakpoints over 50% of the time and on two exhibited more than one breakpoint. Quarry boulders had fewer breakpoints although these occurred at roughly the same point as for outcrop boulders, $\sim$3–5 mm. Only one surface boulder had a breakpoint in roughness scaling (at 1.3 cm).

[43] Hurst exponents, H, are between 0.76 and 0.82 for RMS height and RMS deviation (Table 5). In those boulders with breakpoints, the Hurst exponent ($H2$) was lower at $\sim$0.65. For both RMS height and RMS deviation, quarry boulders had the highest Hurst exponent ($H1$) and outcrop boulders the least, although such small differences fall within the margin of error.

[44] In percent area of morphometric classes, at most scales and for most classes, there were no significant differences ($p < 0.05$) between sites (Table 6, Figure 12). A few exceptions apply, however. At the smallest scale, a window 3 $\times$ 3 pixels corresponding to $\sim$1.5 mm, many significant differences existed between quarry and outcrop boulders and quarry and surface boulders. On average, quarry boulders had more planar classes (64%) than outcrop (52%) or surface (45%) boulders. Surface boulders had more channel features (22%) and ridge features (25%) than the quarry boulders (17% and 17%). Outcrop boulders had more point features (pit, peak, and pass were 1.1%, 1.1%, and 3.5%, respectively), than the quarry boulders (0.5%, 0.5%, 1.5%).

[45] At larger scales, statistically significant differences are fewer. At 1 cm, outcrop boulders had slightly more pits (1.9%) than surface boulders (1.0%). Surface boulders again had more channel features (28%) than quarry boulders (22%). At the 3 cm scale, outcrop boulders had more pass features (10%) than surface boulders (4.4%) (Table 6, Figure 12). At both 3 and 5 cm scales, quarry boulders had more ridges (28% for both scales) than outcrop boulders (18% and 15%).

[46] Variation in class abundance versus scale was also examined to see whether site-specific differences exist (Figure 12). As scale increases, marked differences in percent abundance of features at a single site or differences in rank ordering of sites occasionally occur. For example, while quarry boulders have the fewest pits at the 1.5 mm scale, they have the greatest number of pits at the 5 cm scale. The number of ridge features drops sharply with scale for outcrop boulders while increasing with scale for surface and quarry boulders. The number of pass features on outcrop boulders increases with scale as well.

5. Discussion

[47] Observations and measurements of weathering extent were consistent with the inferred history of the boulders at the 3 sites. The assumption that quarry boulders are relatively ''pristine'' examples of flood-transported debris appears valid. Quarry boulders have characteristic features of flood transport and significantly higher Schmidt hammer rebound values than the other boulders. In thin section, quarry boulders show no signs of chemical alteration, or weathering of the outer mineral grains.

[48] In contrast, boulders at the surface of the Ephrata Fan show signs of extensive breakdown and alteration. The large number of detached rock fragments composing surface

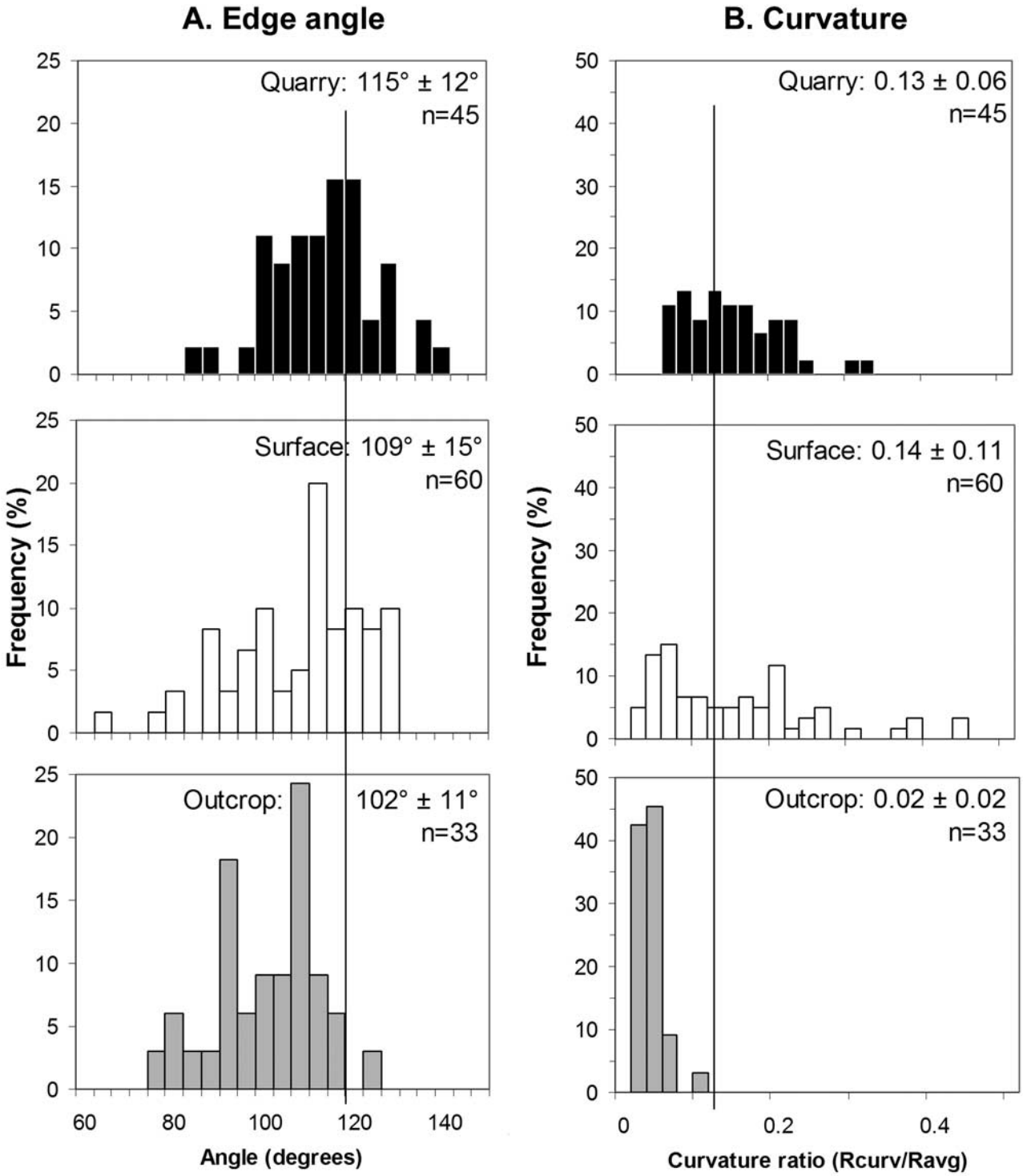

Figure 9. Histograms of frequency distribution of morphometric parameter values at each site. (a) Angle at which facets meet and (b) rounding as measured by radius of curvature ratio. Solid line corresponds to the mean value for the quarry boulders.

boulders and the fact that they have the lowest Schmidt hammer rebound values are consistent with their greater exposure time and in situ breakdown [*McCarroll*, 1991; *Boelhouwers et al.*, 1999]. Surface boulders also show the greatest variation in Schmidt hammer values, consistent with influences from variation in lichen cover which in turn is influenced by factors including rock type, texture, aspect, and moisture availability. Decreased hardness correlates with increased lichen cover, and thus, lichen cover may accelerate weathering as has been shown at other sites [e.g., *Stretch and Viles*, 2002]. Thin sections show lichen assist grain displacement and oxidation of iron-bearing minerals.

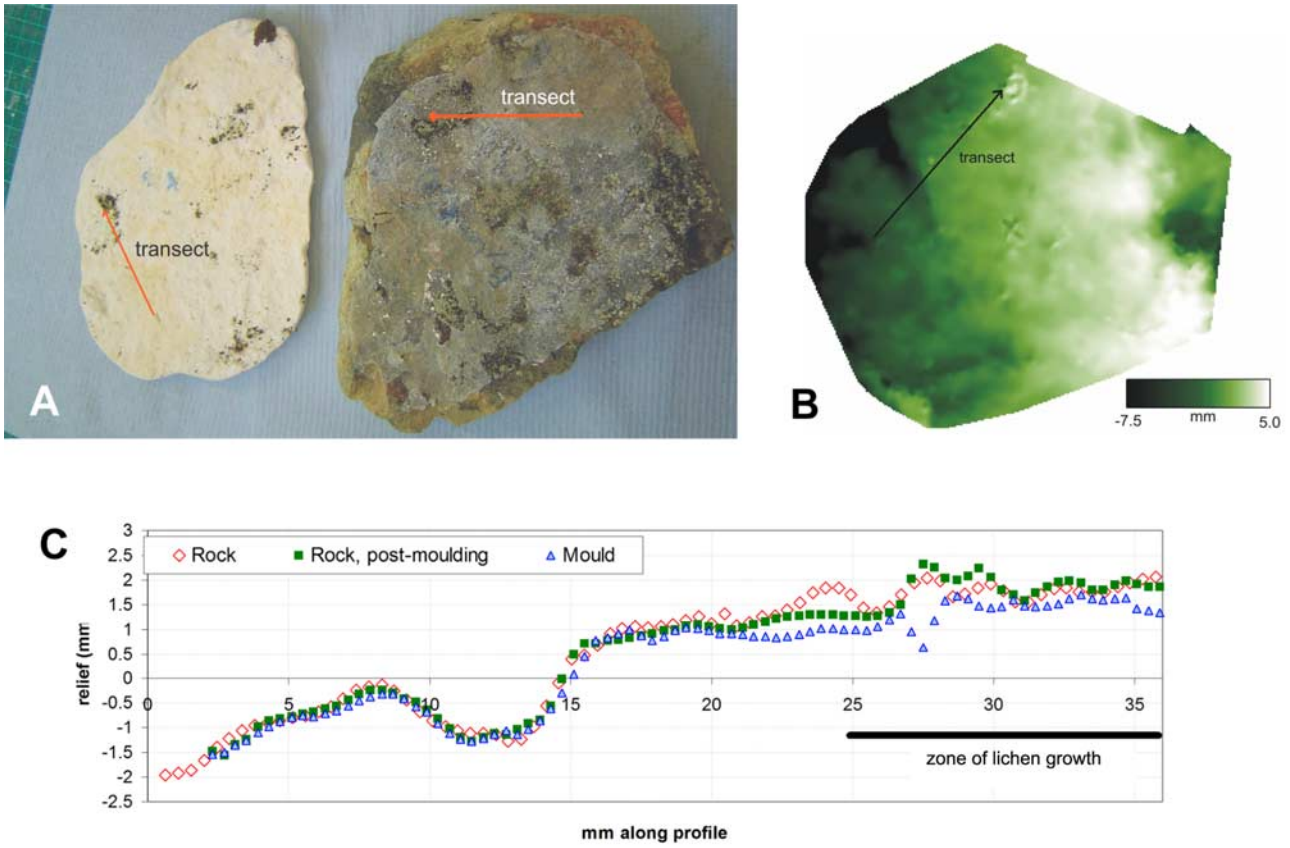
A
transect
transect
B
transect
-7.5
mm
5.0
C
Rock
Rock, post-moulding
Mould
relief (mm
mm along profile
zone of lichen growth
D
rock
rock, post-molding
mold
r.m.s. deviation, log (mm)
step size, log (mm)

Figure 10

Table 4. Summary Statistics for Surface Roughness as a Function of Scale for Boulder Molds[a]

	RMS Height, mm		RMS Slope, °	
	1 mm	1 cm	1 mm	1 cm
Quarry	0.53 ± 0.27	2.58 ± 1.43	12.9 ± 5.7	7.9 ± 4.9
Outcrop	0.76 ± 0.33	3.62 ± 1.26	19.8 ± 11.9	9.9 ± 4.6
Surface	0.86 ± 0.26	4.52 ± 1.71	19.8 ± 9.6	11.3 ± 3.6

[a]Number of samples to compute statistics is listed in Table 5.

Lichens concentrate in depressions on the boulder surface, probably because of the increased moisture trapping potential of topographic lows. These depressions are typically percussion fracture facets from flood transport, suggesting lichen weathering preferentially obscures and degrades these diagnostic morphological features.

[49] Outcrop boulders are intermediate in breakdown extent compared to the quarry and surface boulders in hardness and degree of fracturing. Detached and protruding grains seen in thin section may indicate loss of material through granular disintegration. Hand samples show reddish oxidation from the surface to 1 cm toward the interior on some samples. Others display a banded oxidation zone: a ~1 mm thick band of intense iron staining about 3 mm beneath the rock surface. It is not entirely clear whether this near surface weathering of outcrop boulders occurred before or after detachment from the outcrop.

[50] The boulders' different breakdown paths are recorded by statistically significant morphological differences. Similarity between sites in the macroscopic shape of the boulders indicates that the initial fracture pattern of the parent rock probably controls their moderately "compact" appearance. Parameters for size, edge angle, and radius of curvature were more helpful than *Sneed and Folk*'s [1958] maximum projection sphericity, deviation from compactness, and form factors in providing information which enabled boulders of the three sites to be distinguished. Of all morphological measurements considered, rounding as measured from radius of curvature is the clearest morphological indicator of flood transport with nearly an order of magnitude more rounding in quarry and surface samples as compared to outcrop talus (Table 3, Figure 9b). The existence of some facets with poorly rounded edges among the surface boulders (Figure 9a) is consistent with ongoing breakdown producing fresh, unrounded fractures, like those in outcrop talus.

[51] Roughly equivalent sizes for the outcrop columns and the quarry and surface boulders may reflect boulder formation by plucking of floodwaters exploiting preexisting columnar fractures in the basalt outcrop colonnade [*Baker*, 1978b]. Size sorting during fluvial transport did not significantly influence size over the 6 km separating the quarry and surface site.

[52] Average boulder edge angles for the quarry boulders (Table 3) compare remarkably well to the 120° theoretical mean angle for fracturing during production of hexagonal basalt columns during lava flow cooling [*Lyle*, 2000]. Average values <120° are consistent with measured angles reflecting a combination of preexisting fractures (such as those in hexagonal columnar basalt) and horizontal fractures in the outcrop, perhaps related to unloading (Figure 6c). During initial plucking of boulders from the outcrop, breaks would be primarily along hexagonal columnar joints where cavitation could dislodge fragments. Subsequent posttransport fracturing of flood-transported boulders under the current weathering regime on the fan surface seems to instead release boulder fragments along perpendicular fracture angles. This is reflected in the "tail" of low values in the frequency distribution of edge angle values (Figure 9a).

[53] Outcrop talus boulder shape parameter values are significantly different from those of flood-transported boulders in all aspects. Talus boulders are significantly smaller in comparison to both other boulders and hexagonal column width. Further, talus boulder edges meet at angles far smaller than 120°. Both of these facts are consistent with a different formation mechanism than plucking by floodwaters along columnar fractures. Instead, fractures at a smaller scale are created or preexisting features are propagated until the blocks are released. This was not an expected result but is revealed by examination of the quantitative morphologic parameters. We speculate that a single surface weathering process, recently or presently active, is responsible for detachments which both create the outcrop boulders and cause the surface boulders to fracture in situ. This process creates characteristic 90° angles for fragments typically a few tens of centimeters in size. The present regional climate suggests freeze-thaw cycling as one possible mechanism. Ice segregation could lead to fracture along preexisting joints of rock weakness [*Hallet et al.*, 1991]. Alternatively, moisture percolating along jointing planes might have assisted chemical weathering, weakening the basalt by altering minerals to clays, forming zones of alteration particularly susceptible to failure [*McGreevy*, 1982]. Insolation weathering also can fracture boulders. Cracks formed from these have a specific orientation related to incident solar insolation [*McFadden et al.*, 2005]. To test whether one of these processes is responsible for the most recent morphological imprint from weathering on both surface and outcrop boulders, further variables must be assessed in field study at the Ephrata Fan in relation to the parameters. These include rock temperature variation

Figure 10. (a) Photograph of the control boulder (right) taken postmolding and next to its plaster mold (left). Note photograph was taken angled from normal viewing. Gridlines in the upper left of the photo have centimeter spacing. The transect is labeled. (b) Digital elevation model at 0.5 mm spacing of the control mold. DEM values have been inverted so features match the orientation of the original surface. The x in the DEM center was an indentation left by a marker pen. (c) Profile taken from digital elevation models of the original rock surface, the plaster mold, and the rock surface postmolding. The zone where lichen interfere with accurate recording of elevations is indicated. (d) RMS deviation as a function of scale for the surface of the control rock, the rock surface after casting with plaster, and the mold. *H* values are the same for the original rock and the mold; breakpoint location may differ ~1 mm or less.

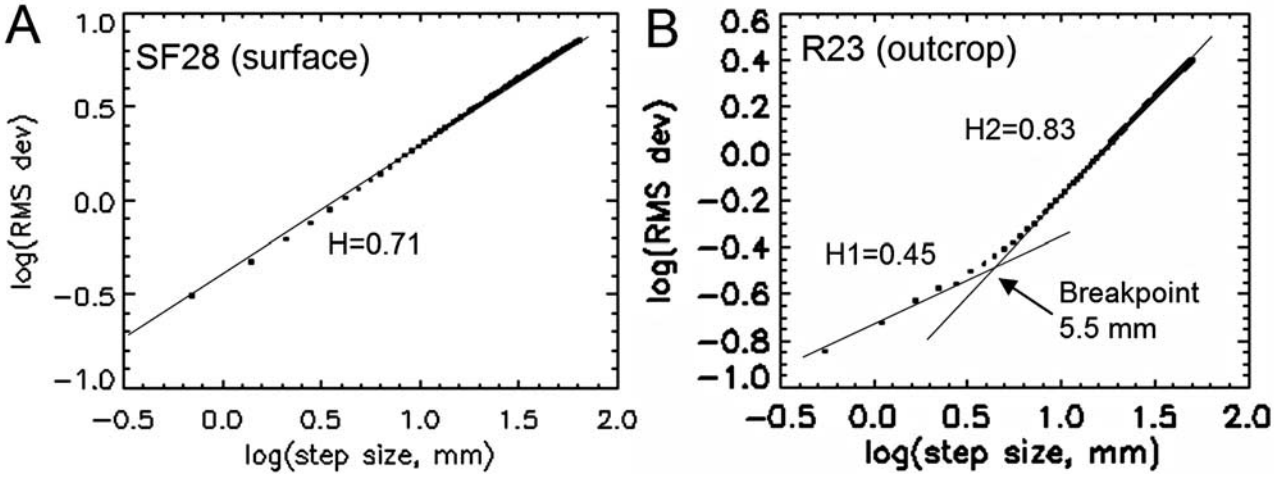

Figure 11. Sample deviograms from boulder surface digital elevation models from (a) a surface boulder mold (SF28) and (b) an outcrop boulder mold (R23). RMS deviation in millimeters is plotted in a log-log plot against the step size in millimeters. The Hurst exponent, *H*, corresponds to the slope of the line and indicates the rate at which roughness increases in the vertical direction as scale increases in the horizontal direction. In Figure 11b there is a breakpoint in scaling behavior at 5.5 mm indicating that different roughening scaling behavior exists at different scales.

seasonally and diurnally, alteration mineral distribution, and aspect of existing cracks and fractures.

[54] Incorporation of surface textural parameters provided a way to distinguish between the two flood-transported boulder populations, which was not possible considering only shape parameters. Both fractal and morphometric classification may thus be useful in assessing weathering processes and timescales. A lesson learned in acquiring boulder textural data is that future studies should generate DEMs directly from rock surfaces [e.g., *Bourke et al.*, 2008]. An artificial reduction in absolute roughness was a limitation we discovered for the molding technique. A possible explanation for the smoothness of both the cast and rock postcast in comparison to the pretreatment rock is disturbance of the uppermost millimeter of the original rock surface. Material on the original boulder may have been compressed or removed during application and peeling of the plaster. Consequently, the collected textural data set is not ideal for direct comparison with stereo data sets of rock surfaces from other sites. RMS height and deviation are likely biased lower and, therefore, in morphometric analysis, more planar features and fewer point classes (pit, peak, pass) are likely to be identified. Nevertheless, the textures of boulders at the Ephrata site can still be compared to each other with a high degree of confidence. Further, Hurst exponent and breakpoint behavior of roughness do not appear different in the rock surface versus the mold for the control rock, indicating these are likely accurate in an absolute sense.

[55] In RMS height and deviation values, quarry boulders are the smoothest and surface boulders are the roughest at all scales. This is consistent with the hypothesis that flood transported boulders were smoothed in transport but (re)roughened as breakdown proceeds in situ. Length of time of surface exposure may be proportional to roughness over the tens of thousands of years time period under consideration at the Ephrata fan. Assumed recent outcrop talus fall is smoother than boulders of the fan surface at all scales except 1 mm where they are roughly equivalent.

[56] Hurst exponent values ($H1$) may theoretically be in the range $0 \leq H \leq 1$. Hurst exponent values of $\sim$0.8 from Ephrata boulders are higher than values previously reported in the literature for topographic surfaces at much larger scales such as lava plains and lava flows (<0.7) [*Shepard et al.*, 2001]. However, this is not entirely surprising since the role of gravity in smoothing surfaces through mass wasting and erosion is more significant at meter to kilometer scales than at the submeter scales considered here.

Table 5. Summary Statistics for Fractal Behavior of Boulder Molds

		Hurst Exponent Behavior[a]			Breakpoint Behavior[b]			
	N (Deviation, Height)	$H1_{dev}$	$H2_{dev}$	$H1_{ht}$	Percent With Breakpoint	Percent With 2+ Breakpoints	Average Breakpoint 1 Scale, mm	Average Breakpoint 2 Scale, mm
Quarry	10, 10	0.80 ± 0.06	0.66 ± 0.07	0.82 ± 0.07	30	0	4.73 ± 1.76	–
Outcrop	9, 10	0.78 ± 0.06	0.63 ± 0.15	0.76 ± 0.05	56	22	3.26 ± 2.04	4.6
Surface	8, 10	0.79 ± 0.05	0.74	0.79 ± 0.06	13	0	13.18	–

[a]Here dev refers to the values from RMS deviation, and ht refers to the breakpoint value from plots of RMS height as a function of window size.
[b]Breakpoint behavior was determined from plots of RMS deviation since no breakpoints were observed over the sampling interval for RMS height.

Table 6. Percent Frequency of Morphologic Classes in Morphometric Classifications for Different Sites and $n \times n$ Window Sizes

		Percentage					
	Scale, mm	Pit	Channel	Pass	Ridge	Peak	Planar
Quarry	1.5	0.5 ± 0.2	16.4 ± 4.9	1.5 ± 0.3	16.9 ± 5.3	0.5 ± 0.1	64 ± 10.0
Quarry	10	1.4 ± 0.9	21.9 ± 4.7	4.7 ± 3.3	24.8 ± 6.6	1.5 ± 0.8	45.7 ± 9.2
Quarry	30	2.9 ± 1.5	25.5 ± 5.9	6.9 ± 4.2	28.0 ± 8.3	1.9 ± 1.7	34.7 ± 9.6
Quarry	50	5.3 ± 5.1	27.6 ± 7.3	10.9 ± 6.4	28.5 ± 8.1	2.9 ± 2.6	24.8 ± 9.2
Outcrop	1.5	1.1 ± 0.4	21.5 ± 5.0	3.5 ± 1.4	20.9 ± 4.7	1.1 ± 0.5	52.0 ± 10.8
Outcrop	10	1.9 ± 0.9	26.3 ± 4.0	6.0 ± 2.7	23.9 ± 5.4	1.6 ± 0.7	40.3 ± 7.5
Outcrop	30	2.9 ± 1.6	29.6 ± 7.1	10.2 ± 4.8	18.4 ± 8.2	2.5 ± 2.4	36.4 ± 10.6
Outcrop	50	4.5 ± 3.4	31.0 ± 16.9	18.3 ± 16.2	15.2 ± 12.9	2.7 ± 3.2	28.3 ± 9.8
Surface	1.5	0.7 ± 0.4	25.2 ± 7.8	2.5 ± 1.2	25.3 ± 7.8	0.8 ± 0.4	45.4 ± 15.1
Surface	10	1.0 ± 0.6	28.1 ± 5.5	4.4 ± 3.2	27.4 ± 8.6	1.5 ± 0.9	37.5 ± 10.5
Surface	30	2.0 ± 3.2	30.0 ± 15.0	4.4 ± 2.9	30.3 ± 14.8	2.2 ± 1.5	31.0 ± 9.4
Surface	50	3.2 ± 6.2	28.9 ± 21.7	5.5 ± 3.9	32.1 ± 19.7	3.8 ± 3.9	26.5 ± 13.9

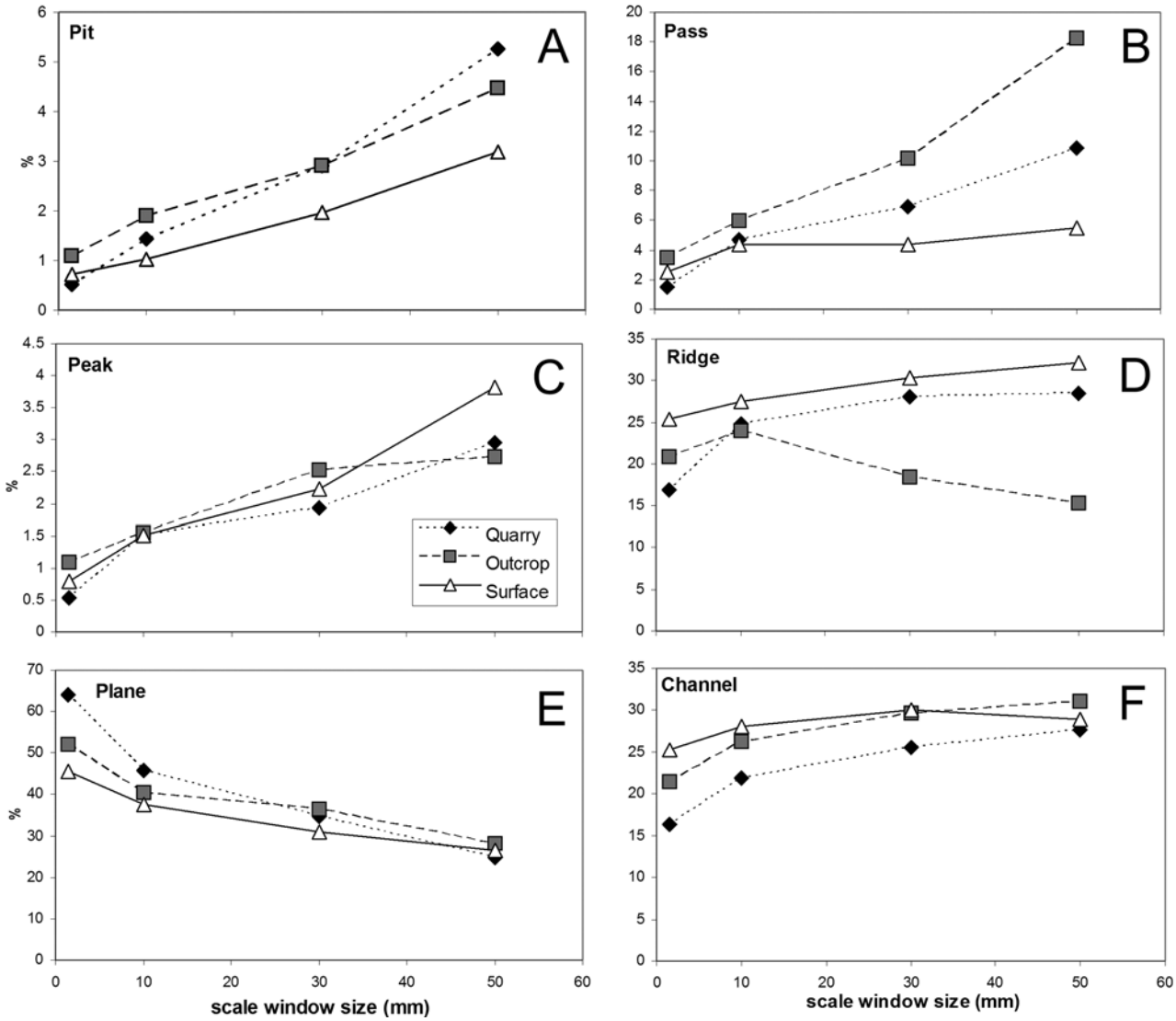

Figure 12. Area percent frequency of morphometric classes as a function of scale window size used. Note y axes vary between plots. Classes are (a) pit, (b) pass, (c) peak, (d) ridge, (e) plane, and (f) channel. Triangles indicate surface boulders, diamonds indicate quarry boulders, and squares indicate outcrop boulders.

[57] Boulder breakpoint behavior is also intriguing if in fact breakpoints indicate changes in the dominance of multiple surface-shaping processes [*Shepard et al.*, 2001]. Most surface boulders had no breakpoints, while at least a third of quarry boulders had breakpoints. This may reflect the fact that the surface texture of quarry boulders results from breakdown action at two distinct scales during fluvial transport: submillimeter smoothing of the surface by abrading sand grains and greater than centimeter-size roughness enhancement via collisions with larger entrained particles to create sharp percussion features. In contrast, boulders exposed at the surface may already have had signatures from these competing processes erased or degraded by dominance of surficial weathering processes which do not generate scale-dependent signatures over millimeter to centimeter. These conclusions about the meaning of fractal parameters are necessarily speculative since, to our knowledge, the millimeter-scale roughness of rock surfaces has only infrequently been measured with respect to weathering [e.g., *McCarroll and Nesje*, 1996] and not previously using this technique.

[58] Morphometric class abundance textural analysis bears out the interpretation from fractal roughness parameters. At small scales, quarry boulders are relatively featureless, dominated by planar features. This agrees with observations of quarry boulder samples in cross section and is consistent with fractal analysis data and the smoothing of the boulders during flood transport and subsequent lack of weathering to further alter the surface. The increased number of ridges on surface and quarry boulders (but not outcrop boulders) at the few centimeters scale may be due to the fact that sharply outlined centimeter-size percussion features resulting from fluvial transport (percussion fracture facets, ridges and terminations, for example) are being detected. Greater roughness of the surface boulders is expressed in channels and ridges, perhaps because of "dissection" of the surface by water where grains are more easily weathered, making these preferred flow paths during rainfall and creating micro channels. Outcrop boulders also have rougher texture than quarry boulders, expressed in greater numbers of pits, peaks, and passes. This might result from inherent roughness of the fracture planes of the rock.

[59] The reduced number of significant differences between sites in terms of morphometric class abundance at larger (few centimeters) scales most likely results from the fact that sample size decreases as scale increases for the $\sim$15 cm $\times$ $\sim$15 cm molds. Sampling larger surface areas and sampling more boulders would improve the data set. The sharp increase in the number of pass features on outcrop boulders with increasing scale may be because small scale (centimeter or less) pit features are classified as pass features at higher (few centimeters) scales when larger window sizes are used for class assignation.

[60] A final consideration is whether these parameters would have been useful in identifying distinct populations of boulders if it were not known, a priori, that there were boulders with three distinct weathering histories. This situation might be typical of an alluvial fan or outwash plain, containing boulders of different ages and lithologies and has arisen in considering the origin of boulders at the Mars Pathfinder landing site [e.g., *Basilevsky et al.*, 1999]. To address this question, principal component analysis (PCA) was performed using six boulder morphologic parameters: long axis, radius of curvature ratio (R_c/R_a), average edge angle, RMS height at 1 mm, RMS height at 1 cm, and $H1$ from RMS height. These were the parameters which produced significant differences among the Ephrata boulders in t tests for site to site differences (plus $H1$ to provide a parameter for roughness scaling behavior). In the PCA, the correlation matrix was used in all calculations to standardize the mean and variance of data. The six computed principal components explain 32%, 30%, 16%, 13%, 5%, and 3% of the variance, respectively. Boulders from the three sites do tend to cluster spatially (Figure 13). Moreover, from plots of the reprojected parameters and data for the first, second, and third components, it is apparent that the shape parameters (long axis, R_c/R_a, and edge angle) contain different information about the boulders than the surface textural parameters based on RMS height. Shape parameters distinguish flood-transported from nonflood-transported boulders while the textural parameters differentiate surface weathered boulders from those which have not been surface weathered. This suggests that to fully explain the natural variation in boulder morphology, it is critical that any quantitative parameter set employ metrics to describe both shape and texture. These different types of morphological data may record evidence from different types of processes.

[61] At present, the shape and textural parameters readily distinguish between flood-transported and talus populations. It is apparent, however, that some overprinting of flood transport signatures is occurring under the surface weathering regime. Percussion marks are being degraded by lichen on surface boulders and continuing fracturing changes the nature of facet angles and curvature. The timescales required for complete overprinting at this site must, however, be far greater than the 10^4 years which have passed since the boulders were transported.

6. Conclusions

[62] A comprehensive parameter set that quantifies complete boulder morphology (size, shape and surface texture) has been successfully developed and tested in this study. Size was measured by lengths of the boulder axes. Shape was calculated using standard sedimentological scales for form [*Sneed and Folk*, 1958] coupled with measures of the angles and radii of curvature of facet edges. Digital models of surface texture were parameterized by measuring fractal scaling of roughness and by morphometric classification.

[63] Using combinations of the parameters, three populations of boulders at the Ephrata Fan site were distinguished: (1) compact boulders with highly curved edges meeting at angles of 115° whose surfaces were smooth at all scales, with some few centimeter-scale ridge and pit features; (2) compact boulders with mostly highly curved edges meeting at angles with median value 115° (and a tail of lower values) and with a rough surface texture exhibiting continuous scaling behavior; and (3) smaller compact boulders with very low curvature edges, whose edge angles had bimodal peaks near 90° and 115°, and whose surfaces were rough but exhibited discontinuous scaling behavior with large numbers of ridges and peaks identified at centimeter scale or less.

Rotman assisted in the preparation and interpretation of thin sections. This work was partly funded by NASA Planetary Geology and Geophysics grant NNG05GJ91G and by the Rhodes Trust.

References

Arvidson, R. E., et al. (2006), Overview of the Spirit Mars Exploration Rover Mission to Gusev Crater: Landing site to Backstay Rock in the Columbia Hills, *J. Geophys. Res.*, *111*, E02S01, doi:10.1029/2005JE002499.

Aydin, A., and J. M. Degraff (1988), Evolution of polygonal fracture patterns in lava flows, *Science*, *239*, 471–476, doi:10.1126/science.239.4839.471.

Baker, V. (1978a), Quaternary geology of the Channeled Scabland and adjacent areas, in *The Channeled Scabland: A Guide to the Geomorphology of the Columbia Basin, Washington*, edited by V. Baker and D. Nummedal, pp. 59–79, NASA, Washington, D. C.

Baker, V. (1978b), Large-scale erosional and depositional features of the channeled scabland, in *The Channeled Scabland: A Guide to the Geomorphology of the Columbia Basin, Washington*, edited by V. Baker and D. Nummedal, pp. 81–116, NASA, Washington, D. C.

Baker, V., and D. Nummedal (Eds.) (1978), *The Channeled Scabland: A Guide to the Geomorphology of the Columbia Basin, Washington*, 186 pp., NASA, Washington, D. C.

Barrett, P. J. (1980), The shape of rock particles: A critical review, *Sedimentology*, *27*, 291–303, doi:10.1111/j.1365-3091.1980.tb01179.x.

Basilevsky, A. T., W. J. Markiewicz, N. Thomas, and H. U. Keller (1999), Morphologies of rocks within and near the Rock Garden at the Mars Pathfinder landing site, *J. Geophys. Res.*, *104*(E4), 8617–8636, doi:10.1029/1998JE900039.

Birkeland, P. W. (1999), *Soils and Geomorphology*, 448 pp., Oxford Univ. Press, New York.

Boelhouwers, J., A. De Joode, and D. Jager (1999), Relative-age dating of debris flow deposits in the Cederberg, *S. Afr. Geogr. J.*, *81*, 135–142.

Bolongaro-Crevenna, A., V. Torres-Rodriguez, V. Sorani, D. Frame, and M. A. Ortiz (2005), Geomorphometric analysis for characterizing landforms in Morelos State, Mexico, *Geomorphology*, *67*(3–4), 407–422, doi:10.1016/j.geomorph.2004.11.007.

Bourke, M., H. Viles, J. Nicoli, P. Lyew-Ayee, R. Ghent, and J. Holmlund (2008), Innovative applications of laser scanning and rapid prototype printing to rock breakdown experiments, *Earth Surface Processes Landforms*, doi:10.1002/esp.1631, in press.

Bourke, M. C., and H. A. Viles (Eds.) (2007), *A Photographic Atlas of Rock Breakdown Features in Geomorphic Environments*, 81 pp., Planet. Sci. Inst., Tucson, Ariz.

Bretz, J. H. (1923), The Channeled Scabland of the Columbia Plateau, *J. Geol.*, *31*, 617–649.

Buffin-Bélanger, T., I. Reid, S. Rice, J. H. Chandler, and J. Lancaster (2003), A casting procedure for reproducing coarse-grained sedimentary surfaces, *Earth Planet. Sci. Lett.*, *28*(7), 787–796.

Clague, J. J., R. Barendregt, R. J. Enkin, and F. Foit Jr. (2003), Paleomagnetic and tephra evidence for tens of Missoula floods in southern Washington, *Geology*, *31*(3), 247–250, doi:10.1130/0091-7613(2003)031<0247:PATEFT>2.0.CO;2.

Curran, J., B. Smith, and P. Warke (2002), Weathering of igneous rocks during shallow burial in an upland peat environment: observations from the Bronze Age Copney Stone Circle Complex, Northern Ireland, *Catena*, *49*, 139–155, doi:10.1016/S0341-8162(02)00023-1.

Day, M. J., and A. S. Goudie (1977), Field assessment of rock hardness using the Schmidt test hammer, *Tech. Bull. Br. Geomorphol. Res. Group*, *18*, 19–29.

Dincer, I., A. Acar, I. Cobano, and Y. Uras (2004), Correlation between Schmidt hardness, uniaxial compressive strength, and Young's modulus for andesites, basalts, and tuffs, *Bull. Eng. Geol. Environ.*, *63*(2), 141–148, doi:10.1007/s10064-004-0230-0.

Dowman, E. A. (1970), *Conservation in Field Archaeology*, 170 pp., Methuen, London.

Durian, D. J., H. Bidead, P. Duringer, A. Schroder, and C. M. Marques (2006), What is in a pebble shape?, *Phys. Rev. Lett.*, *97*, 028001, doi:10.1103/PhysRevLett.97.028001.

Evans, I. S., and C. J. McClean (1995), The land surface is not unifractal: Variograms, cirque scale and allometry, *Z. Geomorphol. Suppl.*, *101*, 127–147.

Fisher, P., J. Wood, and T. Cheng (2004), Where is Helvellyn? Fuzziness of multi-scale landscape morphometry, *Trans. Inst. Br. Geogr.*, *29*, 106–128, doi:10.1111/j.0020-2754.2004.00117.x.

Golombek, M., and D. Rapp (1997), Size-frequency distributions of rocks on Mars and Earth analog sites: Implications for future landed missions, *J. Geophys. Res.*, *102*(E2), 4117–4130, doi:10.1029/96JE03319.

Gordon, S. I., and R. I. Dorn (2005), In-situ weathering rind erosion, *Geomorphology*, *67*(1–2), 97–113, doi:10.1016/j.geomorph.2004.06.011.

Graham, D. J., and N. G. Midgley (2000), Graphical representation of particle shape using triangular diagrams: An Excel spreadsheet method, *Earth Surf. Processes Landforms*, *25*(13), 1473–1477, doi:10.1002/1096-9837(200012)25:13<1473::AID-ESP158>3.0.CO;2-C.

Greeley, R., N. T. Bridges, R. O. Kuzmin, and J. E. Laity (2002), Terrestrial analogs to wind-related features at the Viking and Pathfinder landing sites on Mars, *J. Geophys. Res.*, *107*(E1), 5005, doi:10.1029/2000JE001481.

Grolier, M. J., and J. W. Bingham (1971), Geologic map and sections of parts of Grant, Adams, and Franklin Counties, Washington, *Misc. Geol. Invest. Map I-589*, scale 1:62,500, U.S. Geol. Surv., Dep. of Inter., Washington, D. C.

Hallet, B., J. S. Walder, and C. W. Stubbs (1991), Weathering by segregation ice growth in microcracks at sustained sub-zero temperatures: Verification from an experimental study using acoustic emissions, *Permafrost Periglacial Processes*, *2*, 283.

Heslop, E. E. M., H. A. Viles, and M. C. Bourke (2004), Understanding rock breakdown on Earth and Mars: Geomorphological concepts and facet mapping methods, *Lunar Planet. Sci.* [CD-ROM], *XXXV*, abstract 1445.

Hooper, P. R. (2000), Chemical discrimination of Columbia River basalt flows, *Geochem. Geophys. Geosyst.*, *1*, doi:10.1029/2000GC000040.

Hooper, P. R., V. Camp, S. Reidel, and M. Ross (2007), The origin of the Columbia River flood basalt province: Plume versus nonplume models, in *Plates, Plumes, and Planetary Processes*, edited by G. R. Foulger and D. M. Jurdy, *Geol. Soc. of Am. Spec. Pap. 430*, Geol. Soc. of Am., Boulder, Colo.

Lancaster, N. (1995), *Geomorphology of Desert Dunes*, 320 pp., Routledge, New York.

Long, P. E., and B. J. Wood (1986), Structures, textures, and cooling histories of Columbia River basalt flows, *Geol. Soc. Am. Bull.*, *97*, 1144–1155, doi:10.1130/0016-7606(1986)97<1144:STACHO>2.0.CO;2.

Lyle, P. (2000), The eruption environment of multi-tiered columnar basalt lava flows, *J. Geol. Soc. London*, *157*, 715–722.

Mahaney, W. C. (2002), *Atlas of Sand Grain Surface Textures and Applications*, 237 pp., Oxford Univ. Press, Oxford, U. K.

McCarroll, D. (1991), The Schnidt hammer, weathering, and rock surface roughness, *Earth Surf. Processes Landforms*, *16*(5), 477–480, doi:10.1002/esp.3290160510.

McCarroll, D., and A. Nesje (1996), Rock surface roughness as an indicator of degree of rock surface weathering, *Earth Surf. Processes Landforms*, *21*(10), 963–977, doi:10.1002/(SICI)1096-9837(199610)21:10<963::AID-ESP643>3.0.CO;2-J.

McClean, C. J., and I. S. Evans (2000), Apparent fractal dimensions from continental scale digital elevation models using variogram methods, *Trans. GIS*, *4*, 361–378, doi:10.1111/1467-9671.00061.

McFadden, L. D., M. C. Eppes, A. R. Gillespie, and B. Hallet (2005), Physical weathering in arid landscapes due to diurnal variation in the direction of solar heating, *Geol. Soc. Am. Bull.*, *117*(1/2), 161–173, doi:10.1130/B25508.1.

McGreevy, J. P. (1982), Hydrothermal alteration and earth surface rock weathering: A basalt example, *Earth Surf. Processes Landforms*, *7*, 189–195, doi:10.1002/esp.3290070211.

Mehringer, P. J., Jr. (1985), Late-Quaternary pollen records from the interior Pacific Northwest and northern Great Basin of the United States, in *Pollen Records of Late-Quaternary North American Sediments*, edited by V. M. Bryant Jr. and R. G. Holloway, pp. 167–187, Am. Assoc. of Stratigr. Palynol., Dallas, Tex.

Noormets, R., E. A. Felton, and K. A. W. Crook (2002), Sedimentology of rocky shorelines: 2. Shoreline megaclasts on the north shore of Oahu, Hawaii—Origins and history, *Sediment. Geol.*, *150*, 31–45, doi:10.1016/S0037-0738(01)00266-4.

Rice, J. W., Jr., and K. S. Edgett (1997), Catastrophic flood sediments in Chryse Basin, Mars, and Quincy Basin, Washington: Application of sandar facies model, *J. Geophys. Res.*, *102*(E2), 4185–4200, doi:10.1029/96JE02824.

Richardson, K., and P. A. Carling (2005), A typology of sculpted forms in bedrock channels, *Geol. Soc. Am. Spec. Pap. SPE392*, Geol. Soc. of Am., Boulder, Colo.

Rouai, M., and A. Dekayir (2001), Caractérisation fractale de la porosité d'un basalte altéré, *C. R. Acad. Sci. Ser. 2*, *332*(10), 595–600.

Ryan, R. J., A. M. O'Beirne-Ryan, and M. Zentilli (2005), Rounded cobbles that have not travelled far: Incorporation of coresotones from saprolites in the South Mountain area of southern Nova Scotia, Canada, *Sedimentology*, *52*, 1109–1121, doi:10.1111/j.1365-3091.2005.00730.x.

Sak, P. B., D. M. Fisher, T. W. Gardner, K. Murphy, and S. L. Brantley (2004), Rates of weathering rind formation on Costa Rican basalt, *Geochim. Cosmochim. Acta*, *68*(7), 1453–1472, doi:10.1016/j.gca.2003.09.007.

Shepard, M. K., R. A. Brackett, and R. E. Arvidson (1995), Self-affine (fractal) topography: Surface parameterization and radar scattering, *J. Geophys. Res.*, *100*(E6), 11,709–11,718, doi:10.1029/95JE00664.

Shepard, M. K., B. A. Campbell, M. H. Bulmer, T. G. Farr, L. R. Gaddis, and J. J. Plaut (2001), The roughness of natural terrain: A planetary and remote sensing perspective, *J. Geophys. Res.*, *106*(E12), 32,777–32,796, doi:10.1029/2000JE001429.

Smith, J. A., R. C. Finkel, D. L. Farber, D. T. Rodbell, and G. O. Seltzer (2005), Preservation and boulder erosion in the tropical Andes: Interpreting old surface exposure ages in glaciated valleys, *J. Quat. Sci.*, *20*(7–8), 735–758, doi:10.1002/jqs.981.

Sneed, E. D., and R. L. Folk (1958), Pebbles in the lower Colorado River, Texas: A study in particle morphogenesis, *J. Geol.*, *66*(2), 114–150.

Stretch, R., and H. A. Viles (2002), Lichen weathering on Lanzarote lava flows, *Geomorphology*, *47*, 87–94, doi:10.1016/S0169-555X(02)00143-5.

Sumner, P., and W. Nel (2002), The effect of rock moisture on Schmidt hammer rebound: Tests on rock samples from Marion Island and South Africa, *Earth Surf. Processes Landforms*, *27*, 1137–1142, doi:10.1002/esp.402.

Swanson, D. A., and T. L. Wright (1978), Bedrock geology of the Northern Columbia Plateau and adjacent areas, in *The Channeled Scabland: A Guide to the Geomorphology of the Columbia Basin, Washington*, edited by V. Baker and D. Nummedal, pp. 37–57, NASA, Washington, D. C.

Swanson, D. A., T. L. Wright, P. R. Hooper, and R. D. Bentley (1979), Revisions in stratigraphic nomenclature of the Columbia River Basalt Group, *U.S. Geol. Surv. Bull. 1457-G*, 59 pp., U.S. Geol. Surv., Washington, D. C.

Tinkler, K. J., and E. E. Wohl (Eds.) (1998), *Rivers Over Rock: Fluvial Processes in Bedrock Channels*, 323 pp., AGU, Washington, D. C.

Turcotte, D. L. (1997), *Fractals and Chaos in Geology and Geophysics*, 414 pp., Cambridge Univ. Press, New York.

Turkington, A. V., and J. D. Phillips (2004), Cavernous weathering, dynamical instability, and self-organization, *Earth Surf. Processes Landforms*, *29*(6), 665–675, doi:10.1002/esp.1060.

Viles, H. A. (2001), Scale issues in weathering studies, *Geomorphology*, *41*, 63–72, doi:10.1016/S0169-555X(01)00104-0.

Williams, G. P. (1983), Paleohydrological methods and some examples from Swedish fluvial environments. part I: Cobble and boulder deposits, *Geogr. Ann. Ser. A*, *65*(3/4), 227–243.

Williams, R. B. G., and D. A. Robinson (1983), The effect of surface texture on the determination of surface hardness of rock using the Schmidt hammer, *Earth Surf. Processes Landforms*, *8*, 289–292, doi:10.1002/esp.3290080311.

Wood, J. (1996), The geomorphological characterisation of digital elevation models, Ph.D. thesis, Univ. of Leicester, Leicester, U. K. (Available at http://www.soi.city.ac.uk/~jwo/phd)

Wyatt, M. B., and H. Y. McSween Jr. (2002), Spectral evidence for weathered basalt as an alternative to andesite in the northern lowlands of Mars, *Nature*, *417*, 263–266, doi:10.1038/417263a.

Yang, Z. Y., and T. J. Wu (2006), An index for describing the core-stone shape in weathered columnar joints, *Geotech. Geol. Eng.*, *24*, 1349–1363, doi:10.1007/s10706-005-2213-8.

Yingst, R. A., A. F. C. Haldemann, K. L. Biedermann, and A. M. Monhead (2007), Quantitative morphology of rocks at the Mars Pathfinder landing site, *J. Geophys. Res.*, *112*, E06002, doi:10.1029/2005JE002582.

M. C. Bourke, Planetary Sciences Institute, 1700 East Fort Lowell, Suite 106, Tucson, AZ 85719, USA.

B. L. Ehlmann, Department of Geological Sciences, Brown University, Box 1846, Providence, RI 02912, USA. (bethany_ehlmann@brown.edu)

H. A. Viles, School of Geography and Environment, University of Oxford, South Parks Road, Oxford OX1 3QY, UK.